TRANSMISSION AMPLITUDE VARIATION WITH OFFSET

(TAVO)

BY

AFEEZ KOLA POPOOLA

A Thesis Presented to the

DEANSHIP OF GRADUATE STUDIES

KING FAHD UNIVERSITY OF PETROLEUM & MINERALS

DHAHRAN, SAUDI ARABIA

In Partial Fulfillment of the
Requirements for the Degree of

MASTER OF SCIENCE

In

GEOPHYSICS

JANUARY, 2014

KING FAHD UNIVERSITY OF PETROLEUM & MINERALS
DHAHRAN 31261, SAUDI ARABIA

DEANSHIP OF GRADUATE STUDIES

This thesis, written by **AFEEZ KOLA POPOOLA** under the direction of his thesis advisor and approved by his thesis committee, has been presented to and accepted by the Dean of Graduate Studies, in partial fulfillment of the requirements for the degree of **MASTER OF SCIENCE IN GEOPHYSICS**.

Thesis Committee

Dr. Abdullatif Al-Shuhail (Advisor)

Dr. Ismail Kaka (Member)

Dr. Khalid Al-Ramadan (Member)

Dr. Abdulaziz Al-Shaibani
Department Chairman

Dr. Salam A. Zummo
Dean of Graduate Studies

30/11/14
Date

عمادة الدراسات العليا
DEANSHIP OF GRADUATE STUDIES

Dedication

To my lovely parents, caring wife and beautiful daughter for their prayers, support and patience.

ACKNOWLEDGMENTS

All praises are due to Allah Almighty for his guidance and blessing, may peace and blessings be upon the noblest of mankind Muhammad (S.A.W). I thank Allah for the patience he granted me to go this far. I am grateful to my parents for their prayers, support and patience. I also thank my wife and daughter for their understanding and cooperation throughout the course of the work and coping with my long absence from home.

I am indebted to my thesis advisor, Dr. Abdullatif Al-Shuhail, whose brilliant idea led to the topic of this thesis. I also thank him for his advices and encouragements throughout this work and his help and assistance in making the objectives achievable. I like to appreciate my committee members, Drs. Ismail Kaka and Khalid Al-Ramadan for their painstaking review of my write-up and helpful suggestions. I especially like to thank Prof. Gabor Korvin who was always happy to answer my questions no matter what it was and for his kindness in carefully checking my equations to ensure their correctness. I would like to thank other people who helped me at the early stages of this work, Dr. Mohammad Badri and Mr. Hammad Tariq of Schlumberger, Dr. Ahmet Tatar, Jan Thorbecke and others. Support from Tesseral Technologies Inc. in Calgary for giving me an evaluation license for the Tesseral software is also appreciated.

A number of people have also made my stay in Saudi Arabia a memorable experience, first I will like to thank Drs. Khalid Al-Ramadan and Ismail Kaka for their moral and financial support for me since my first year at KFUPM, may Allah reward them with good. To the Al-hussaini's family , I will always appreciate your acceptance and support for me and my family, it has been unbelievable, thank you and I pray Allah reward you with what is better. I also thank my former room-mate and friend Saadiq Owodunni for all his support and care. I thank Kareem Lateef for his help with some of the mathematics of this work and sharing some Mathematica programming tips. The support of the Nigerian community in the Kingdom has been unprecedented; I can go on and on, but the list of names will be inexhaustible. I really thank everybody for their love, prayers, encouragement, advice and support for me and my family throughout my sojourn in KFUPM.

I am also grateful to the Saudi government through KFUPM for granting the scholarship to complete my Masters degree. Above all, all praises belong to Allah.

TABLE OF CONTENTS

LIST OF TABLES

LIST OF FIGURES

LIST OF ABBREVIATIONS

$\alpha = (\alpha_2 + \alpha_1)/2$	Average P-wave velocity
$\beta = (\beta_2 + \beta_1)/2$	Average S-wave velocity
$\Delta\alpha = \alpha_2 - \alpha_1$	P-wave velocity difference
$\Delta\beta = \beta_2 - \beta_1$	S-wave velocity difference
$\Delta\rho = \rho_2 - \rho_1$	Density difference
$\rho = (\rho_2 + \rho_1)/2$	Average density
R_{PP}	PP-reflection coefficient
R_{PS}	PS-reflection coefficient
$\theta = (\theta_i + \theta_t)/2$	Average angle
T_{PP}	PP-transmission coefficient
T_{PS}	PS-transmission coefficient
AVO	Amplitude variation with offset
CRG	Common receiver gather
CSG	Common shot gather

FWM	Full-waveform modeling
PP	Incident P-Wave to reflected or transmitted P-Wave
PS	Incident P-Wave to reflected or transmitted S-Wave
$TAVO$	Transmission AVO
VSP	Vertical seismic profiling

THESIS ABSTRACT

NAME: Afeez Kola Popoola

TITLE OF STUDY: TRANSMISSION AMPLITUDE VARIATION WITH OFFSET (TAVO)

MAJOR FIELD: Geophysics

DATE OF DEGREE: January, 2014

Amplitude variation with offset (AVO) has been applied over the years in reservoir geophysics for various applications including fluid detection and lithology typing among others. Existing AVO methods utilize the reflected waves produced when a compressional body wave is incident on an elastic interface. This study presents new approximations for the transmission PP and PS coefficients from Aki and Richards (2002) equations.The new approximations were compared to the original Aki and Richards' approximations using three different published simple reservoir models. The transmission P-wave was approximated by a linear function while the transmission converted S-wave was approximated with a polynomial function.

Results show that there is a similar transmission P-wave amplitude versus offset response for the gas sand models which is different from the oil sand model's re-

sponse. All the three models showed similar trends for the transmission converted S-wave response, which is a general decrease of amplitude with offset. The T_{PS} response was inverted for three elastic parameter contrasts: the average S-wave/P-wave velocity, the density difference/average density and the S-wave velocity difference/average S-wave velocity across the interface. Inversion resulted in a fairly good estimation for two parameters only (the average S-wave/P-wave velocity and the S-wave velocity difference/average S-wave velocity) up to intermediate angle of incidence but failed to recover one of the parameters (density difference/average density) with reasonable accuracy probably due to high non-linearity of the starting T_{PS} equation and high dependence of this parameter on higher order terms in the T_{PS} approximation. The presented approximations are ideal for use with VSP geometry with receivers below the target horizon.

ملخص الرسالة

الاسم الكامل: افيز كولا بوبولا
عنوان الرسالة: التغير في سعة الموجه مع المسافة الجانبية
التخصص: الجيوفيزياء
تاريخ الدرجة العلمية: صفر 1435

الاختلاف في سعة الموجه مع المسافه الجانبية يتم استخدامه منذ فترة طويلة في جيوفزياء المكامن و في تطبيقات متعددة علي سبيل المثال تحديد الموائع و نوع التركيب الليثولجي. اختلاف في سعة الموجه مع المسافه الجانبية تستخدم خاصية الموجه المنعكسة الناتجة من موجة جسمية تضاغطية ساقطة علي حد متمدد فاصل بين سطحيين .

هذه الدراسة تستعرض طريقة جديدة لتقديرو إستنتاج معاملات الامرارية لموجات PP وPS من معادلات Aki و(2002) Richard . هذه التقديرات الجديدة المستنتجة تمت مقارنتها مع تقديرات Aki وRichardباستخدام ثلاثة نماذج لمكامن مختلفة هذه النماذج منشورة في المجلات العلمية.

معامل الامراريه لموجة الاولية تم تقديره بواسطة دالة خطية بينما معامل الامراريه لموجة الثانوية الناتجة تم تقديره بواسطة دالة غير خطية متعددة الحدود.

النتائج اظهرت أن هناللك تشابه في معامل الامرارية بين نموذجيين الذيين يحتويان علي الغاز و الرمل الذيين يختلفان عن النموذج الذي يحتوي علي الرمل و النفط. كل الثلاثة نماذج اظهرت تشابه في الخصائص الامرارية لموجات الثانوية التي تتمثل في نقصان عام في سعة الموجة مع المسافة الجانبية .

الامرارية لموجة PS تم تحويلها إلي ثلاثة معاملات تمدد و هي متوسط سرعة الموجة الثانوية إلي سرعة الموجة الاولية ,الاختلاف في الكثافة بين الحديين الفاصليين إلي متوسط الكثافة و الفرق بين سرعة الموجة الثانوية إلي متوسط سرعة الموجة الثانوية علي امتداد السطح الفاصل هذه العملية التحويلية اظهرت نتائج جيدة في استنتاج معاملين فقط و هما { متوسط سرعة الموجة الثانوية إلي سرعة الموجة الاولية و الفرق بين سرعة الموجة الثانوية إلي متوسط سرعة الموجة الثانوية علي امتداد سطح الفاصل } حتي االزاوية المتوسط لموجه الساقطة ,لكن فشلت في استنتاج معامل الاختلاف في الكثافة بين حديين الفاصليين إلي متوسط االكثافة نتيجة لى لاعتمادها علي دالات ذات معاملات غير خطية بينما الدالة التي اتخدمت ذات معامل خطي.

النتائج المستخلصة في هذه الدراسة يمكن استخدامها في VSP في حالة الجيفونات الموجودة تحت النطاق المستهدف.

CHAPTER 1

INTRODUCTION

1.1 Introduction

In exploring for oil and gas resources, which is presently the major source of fossil fuel in the world, geoscientists employ different methods. Seismic reflection method is the industry's unanimous choice when it comes to hydrocarbon exploration. This is because of its wider coverage at a relatively small amount of time compared to other ground geophysical methods. Borehole seismology is an offshoot of the wider exploration seismology in which seismic signals are recorded by receivers that are lowered downhole (Hardage, 2000). Vertical seismic profiling (VSP) as an example is carried out in an existing borehole, usually an exploration well. In the quest to better understand hydrocarbon reservoirs, a plethora of geophysical techniques to aid interpretation have evolved. One such method is amplitude variation with offset (AVO) which some geoscientists classified into the family of direct hydrocarbon indicators (DHI) (Brown, 2004).

Amplitude variation with offset involves the analysis of the behavior of seismic wave amplitude as a function of the incident angle of the impinging wave which could be directly translated to offset using appropriate geometry. Conventional AVO analysis involves the analysis of the variation in amplitudes of reflected signals with incidence angle and is used in many exploration applications including fluid detection, lithology typing and fracture mapping.

The Zoeppritz equations express the exact plane wave amplitudes of reflected and transmitted waves as functions of angles of incidence and transmission, but do not give an intuitive understanding of how these amplitudes relate to the various physical parameters such as velocity and density. In order to make these important Zoeppritz equations more useful, different approximations have appeared for these equations in the literature, especially for the reflected amplitudes. A first practical approximation to the Zoeppritz equation was made by Bortfeld (1961), after which more approximations were published and used in AVO analysis. The most popular approximation was given by Aki and Richards (2002), which presented a first-order linear approximation of Zoeppritz equations.

Despite successes and limitations of the AVO method, it has become part of the industry standard in seismic data analysis and interpretation for reservoir detection and characterization. Over the years, the use of AVO analysis have been widely applied to surface seismic data. However, in recent years borehole seismic measurements have become widely available to better understand insitu reservoir properties.

In this study, I propose using AVO analysis on VSP data but on transmission rather than reflection amplitudes. The proposed method has the main advantage over classical reflection VSP-AVO analysis of avoiding undesirable effects associated with reflected arrivals because it only utilizes the downgoing (direct) wavefield. These undesirable effects include:

- Amplitude losses by absorption due to traveling through deeper formations with unknown absorption coefficients.
- Amplitude losses due to reflection at deeper interfaces.
- Wavelet non-stationarity by shifting to lower frequencies due to traveling longer (deeper) distances in the Earth, which acts as a low-pass filter.
- Accuracy loss in modeling due to ray bending by velocity heterogeneities in deeper formations.

The thesis is organized into six chapters. Chapter one deals with the background of the proposed problem and the objectives of this study. In chapter two, important previous published works were reviewed. In chapter three, the methodology that has been followed in accomplishing the objectives are discussed, approximations for transmission plane wave into a more practical expression for AVO analysis are shown with the theory and derivation of relevant equations. Various models that have been used to test the approximations are also included. In chapter four, synthetic data were generated through convolutional modeling from the Aki and Richards equations to be used in inverting for the elastic parameters.

Results obtained from modeling and inversion of the transmission amplitudes are discussed in chapter five. Finally, in chapter six, I close with conclusions drawn from the and made some recommendations for future studies.

1.2 Statement of the Problem

The partition of seismic energy/amplitude at an interface is represented in Figure 1.1. Two of the resulting scattered energy are reflected and the other two are transmitted into the underlying layer. Most previous AVO studies have been applied on either only the reflected PP or both reflected PP and PS amplitudes. However, with the proliferation of VSP data, analysis of transmission PP and PS should give us additional information and also eliminates some of the undesirable effects associated with reflected waves. This study will address the use of transmission amplitude variation with offset from VSP data to estimate changes in elastic properties while reducing the undesirable effects associated with current AVO analysis.

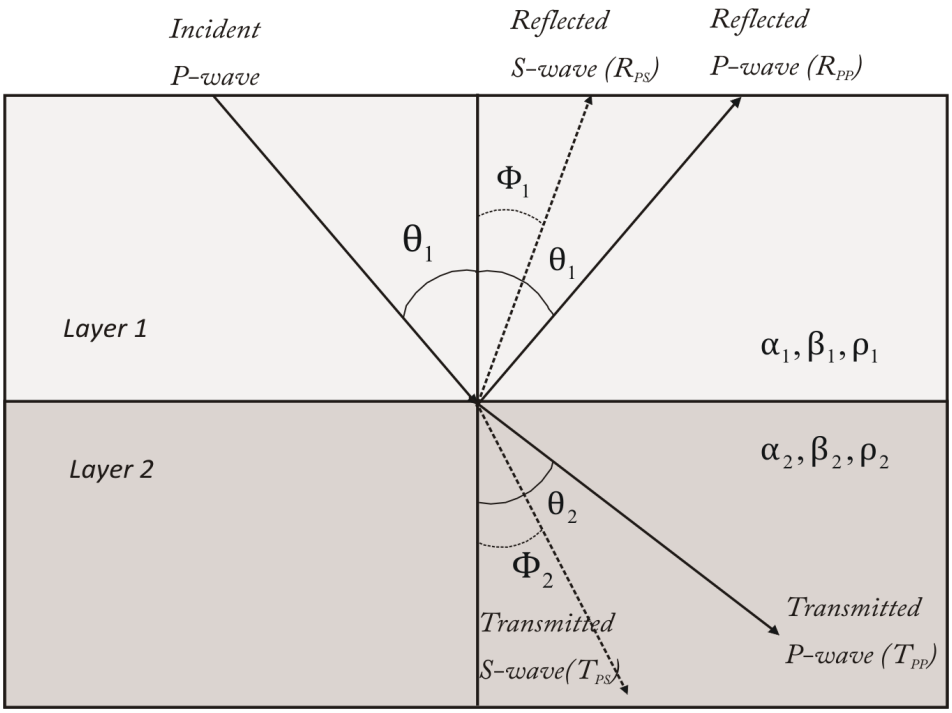

Figure 1.1: Partition of energy at an elastic interface between two half-spaces with reflection and transmission waves

1.3 Objectives

Reflection AVO has been extensively studied with varying applications in reservoir characterization. However, the present study is directed towards applying AVO analysis on transmitted wave amplitudes. Appropriate approximations will be derived that make the transmission AVO analysis similar to the conventional AVO analysis. The approximate equations relating transmission amplitudes to incidence angle will then be inverted for elastic parameter contrasts. The derived approximations are expressed in a way that facilitates their use with existing AVO technologies.

1.4 Advantages of TAVO

High resolution is often sought after in the application of any geophysical technique. Reflection seismic wave arrivals suffer from absorption and other effects due to longer travel path before they are recorded. However, transmitted seismic wave, recorded by VSP geophone, travel shorter distance and more importantly are recorded close to the subsurface formation from which they are generated/scattered. This should lead to higher resolution with transmitted wave amplitude compared to reflections. Therefore, using the amplitudes from these wave arrivals in AVO analysis would probably increase the accuracy of elastic parameter estimation from AVO studies. Transmission AVO method could also be incorporated and used as a tool in conjunction with reflection AVO to increase the confidence in AVO for reservoir identification.

CHAPTER 2

LITERATURE REVIEW

2.1 Zoeppritz equations approximation

The propagation of plane wave incident on an elastic interface results into the partition of the wave's energy between the layers above and below the interface. Figure 1.1 showed a schematic of the four types of wave modes that result from an incident P-wave. Two of the scattered waves at the interface are reflected into the layer above and another two are transmitted into the layer below. The two reflected waves are denoted as R_{PP} and R_{PS} while T_{PP} and T_{PS} denote the transmitted wave modes.

Bortfeld (1961) presented an approximation, using a physical approach, for the reflected and transmitted coefficients for a vertically-incident longitudinal wave because the exact equations are difficult to use. He derived an equation for the reflected wave for an interface from which the effect of the Poissons ratio could be noticed directly. He also observed the dependence of all converted waves on the

shear wave velocity ratio above and below the reflecting interface. In the derivation of the reflection and transmission amplitudes he assumed the incidence angles are smaller than the critical angle and changes in elastic parameters are small as well, and using these assumptions, the amplitude of the transmitted P-wave will only differ from the incident P-wave by a small amount. Bortfeld, following the exact values given by Muskat and Meres (1940) was able to compare his approximations to the exact values and made the following important observations for a typical Poisson solid. First, he noted that, the deviations between his approximations and the exact are not greater than few percent which he did not actually quantify. Second, the deviations increase with increasing incidence angle. Third, the deviations increase with increasing contrasts of the elastic parameters, but noting that the combined contrasts of all elastic parameters plays an important role. Finally, the deviations decrease if the effect of the contrasts are counteracting, for instance $V_1/V_2 > 1$ while $\rho_1/\rho_2 < 1$.

Aki and Richards (2002), provided a starting point for most practical AVO analyses. They approximated the exact Zoeppritzs equation in a simple way in order to attempt an approximation for any wave mode as a function of incidence angle (R_{PP}, R_{PS}, T_{PP}, T_{PS}, R_{SP}, R_{SS}, etc). However, for the approximations to be valid, they made some important assumptions which are to be considered when working with the equations. The assumptions are similar to those made by Bortfeld in his paper. The important ones being that, the changes in elastic parameters are small across the interface and that all angles involved are real and

less than 90°. Aki and Richards (2002) noted that, for waves that retain the same mode across the incidence interface. That is, for an incident P-wave, all other types of scattering (e.g reflected P-wave R_{PP}) coefficient will be small compared to transmission P-wave coefficients, which will be of the order of one for small jumps in density and velocity contrasts. The conversions between P and S are all insensitive to first-order changes in the P-wave speed. The given approximate formulas will fail if any angle is near 90°.

2.2 Applications of the approximations in AVO studies

The work of Ostrander (1984) pioneered the practical use of Zoeppritz equations in exploration. He introduced and explained the phenomenon of reflection amplitude change and how it could serve to characterize a reservoir. He utilized an approximate Zoeppritz equation to analyze the offset dependence variations in reflections amplitude for a simple horizontal three-layer gas sand model. He used a gas and brine saturated sand layers sandwiched between two shale layers. He noticed from the changes in amplitudes as a function of incidence angle that there is a variation in amplitude good enough to differentiate between brine and gas saturated sand using published values of Poissons ratio.

Shuey (1985), popularized the practical application of AVO by introducing an interpretation technique for AVO analysis. He gave a simplification of the

reflected R_{PP} Zoeppritz equations into a three-term equation with each term contributing differently at different angles of incidence. The simplification emphasizes obtaining elastic properties from reflection coefficients at an elastic interface. He described AVO as an inverse problem in which elastic parameters are inferred from the observed amplitude as a function of increasing offset. His approximations for the reflected P-wave differ from that of Bortfeld (1961) in the way each terms were grouped. Considering the initial assumptions of small change in properties and angles less than 90° by Aki and Richards (2002), he noted that in case of velocity decrease his approximation is good only to about 80° and in case of velocity increase, it is good to only about 10° less than the critical angle. The angles in these approximations are the average between the incidence and transmission angles.

Another approximation to R_{PP} and R_{PS} was given by Xu and Bancroft (1997) which presented a joint AVO analysis on R_{PP} and R_{PS} seismic data from Blackfoot, Alberta. They derived some equations for R_{PS} coefficient easier to be used in PS AVO analysis. They utilized the least-square regression analysis to extract elastic parameters from pre-stack seismic data and obtained the R_{PP} coefficient for constant terms in the approximation independent of incidence angle. The difficulties of PS data processing were also discussed. They compared the different approximations for various models and pointed out effects of S-wave changes on different models.

Coulombe et al. (1992, 1996) applied AVO on VSP data. They considered the use of multioffset VSP geometry with a multi-component processing workflow to obtain the reflection coefficients for the purpose of AVO analysis. They used VSP data in order to avoid problems associated with surface seismic methods, while leverage on the qualities of VSPs. They also pointed out the importance of good velocity model as a starting point in obtaining P-wave angle of incidence which may not be so important in surface seismic applications but may overwhelm important subtle effects like AVO. They mentioned that due to the difference in the frequency of operation between the measurements of borehole log and surface seismic, AVO response using sonic velocities may not effectively match surface seismic observations. Thus, VSP measurement provides a good compromise between the two. Also because VSP is recorded in situ, it provides a better understanding of the propagating wavefield, close to the formation of interest.

CHAPTER 3

METHODOLOGY

The method to be followed in this thesis includes getting a suitable approximation for the transmission amplitudes as a function of incidence angle. In order to achieve this, I start from Aki and Richards (2002) approximation of the exact T_{PP} and T_{PS} Zoeppritz equations. These equations will then be expressed as a function of incidence angle only as opposed to dependence on both incidence and refracted angles in the original equations. Since the objective is to analyze the offset/angle dependence of the amplitude of transmitted $T_{PP}(\theta)$ and $T_{PS}(\theta)$ into a form which is convenient and in accordance with current technique for AVO analysis, a linear relation is desired between amplitude and angle of incidence. After achieving this, the approximations were tested on different rock models for assessment by comparing them with the initial Aki and Richards (2002) equations as well as the full Zoeppritz equations.

3.1 Theory

Starting from the approximate expressions given by Aki and Richards (2002) for the transmission amplitude of PP and PS waves as shown in equations 3.1 and 3.2

$$T_{PP} = 1 - \frac{1}{2}\frac{\Delta\rho}{\rho} + \left(\frac{1}{2\cos^2\theta} - 1\right)\frac{\Delta\alpha}{\alpha} \tag{3.1}$$

$$T_{PS} = \frac{p\alpha}{2\cos\phi}\left[\left(1 - 2\beta^2p^2 - 2\beta^2\frac{\cos\theta}{\alpha}\frac{\cos\phi}{\beta}\right)\frac{\Delta\rho}{\rho} - 4\beta^2\left(p^2 + \frac{\cos\theta}{\alpha}\frac{\cos\phi}{\beta}\right)\frac{\Delta\beta}{\beta}\right] \tag{3.2}$$

where p in equation 3.2 is the ray parameter given as;

$$p = \frac{\sin\theta}{\alpha} = \frac{\sin\phi}{\beta} \tag{3.3}$$

approximate expressions will be derived for both T_{PP} and T_{PS} as a function of incidence angle θ.

3.1.1 Derivations of transmission amplitudes

The expressions for amplitudes of transmitted body waves T_{PP} and T_{PS} as a function of the waves' incidence angle as it strikes the elastic interface will be obtained. These expressions will serve as the basis for the estimation of models' elastic parameters change across the interface.

3.1.2 Transmission PP-wave approximation

Equation 3.1 can be expressed in terms of the incident angle θ using the relation: $\sec^2\theta = 1 + \tan^2\theta$

$$T_{PP}(\theta) = \left(1 - \frac{\Delta\rho}{2\rho} - \frac{\Delta\alpha}{2\alpha}\right) + \frac{\Delta\alpha}{2\alpha}\tan^2\theta \tag{3.4}$$

which can be put in the following AVO-convenient form as;

$$T_{PP}(\theta) = A + B\tan^2\theta \tag{3.5}$$

where

$$A = 1 - \left(\frac{\Delta\rho}{2\rho} + \frac{\Delta\alpha}{2\alpha}\right) = 1 - R_{PP0} = T_{PP0} \tag{3.5a}$$

$$B = \frac{\Delta\alpha}{2\alpha} \tag{3.5b}$$

R_{PP0} and T_{PP0} are the zero-offset PP-reflection and transmission coefficients respectively. Figure 3.1(a) shows the plot of transmission PP amplitude as a function of incidence angles for Zoeppritz, Aki-richards and equation 3.4. The parameters used in modeling are shown in Table 3.1.

3.1.3 Transmission PS-wave approximation

For the case of T_{PS} an approach similar to that presented in Donati and Martin (1998) was followed where they expressed R_{PP} as a polynomial series of sines and

cosines. They reported the approximation with polynomial of sine series to be more accurate up to a fairly large incidence angle compared to that of cosine. I chose sine series over cosine for similar reasons. Also, an approximation in which the combinations of the elastic properties have more significance as offset increases is more intuitive when using a sine rather than cosine series. Terms involving the angle ϕ in equation 3.2 can be expressed in terms of the angle θ as:

$$\sin\phi = \frac{\beta}{\alpha}\sin\theta \tag{3.6}$$

$$\cos\phi = \sqrt{1 - \left(\frac{\beta}{\alpha}\right)^2 \sin^2\theta} \tag{3.7}$$

Substituting equations 3.3 and 3.7 into equation 3.2 and expanding in a Maclaurin's series, and then expressing the terms in $\sin\theta$ series yields;

$$\begin{aligned} T_{PS}(\theta) \approx \left[-\frac{\beta}{\alpha}\left(\frac{\Delta\rho}{\rho} + \frac{2\Delta\beta}{\beta}\right) + \frac{1}{2}\frac{\Delta\rho}{\rho}\right]\sin\theta + \left[\frac{\beta}{\alpha}\left(\left(\frac{\Delta\beta}{\beta} + \frac{\Delta\rho}{2\rho}\right) - \frac{\beta}{\alpha}\left(\frac{2\Delta\beta}{\beta} + \frac{3\Delta\rho}{4\rho}\right)\right)\right]\sin^3\theta \\ + \frac{1}{8}\left(\frac{\beta}{\alpha}\left(\frac{2\Delta\beta}{\beta} + \frac{\Delta\rho}{\rho}\right) - \left(\frac{\beta}{\alpha}\right)^4\left(\frac{8\Delta\beta}{\beta} + \frac{5}{2}\frac{\Delta\rho}{\rho}\right)\right)\sin^5\theta \end{aligned} \tag{3.8}$$

which can be put in an AVO-convenient form as;

$$T_{PS}(\theta) \approx C\sin\theta + D\sin^3\theta + E\sin^5\theta \tag{3.9}$$

where

$$C = -\frac{\beta}{\alpha}\left(\frac{\Delta\rho}{\rho} + \frac{2\Delta\beta}{\beta}\right) + \frac{1}{2}\frac{\Delta\rho}{\rho} \tag{3.9a}$$

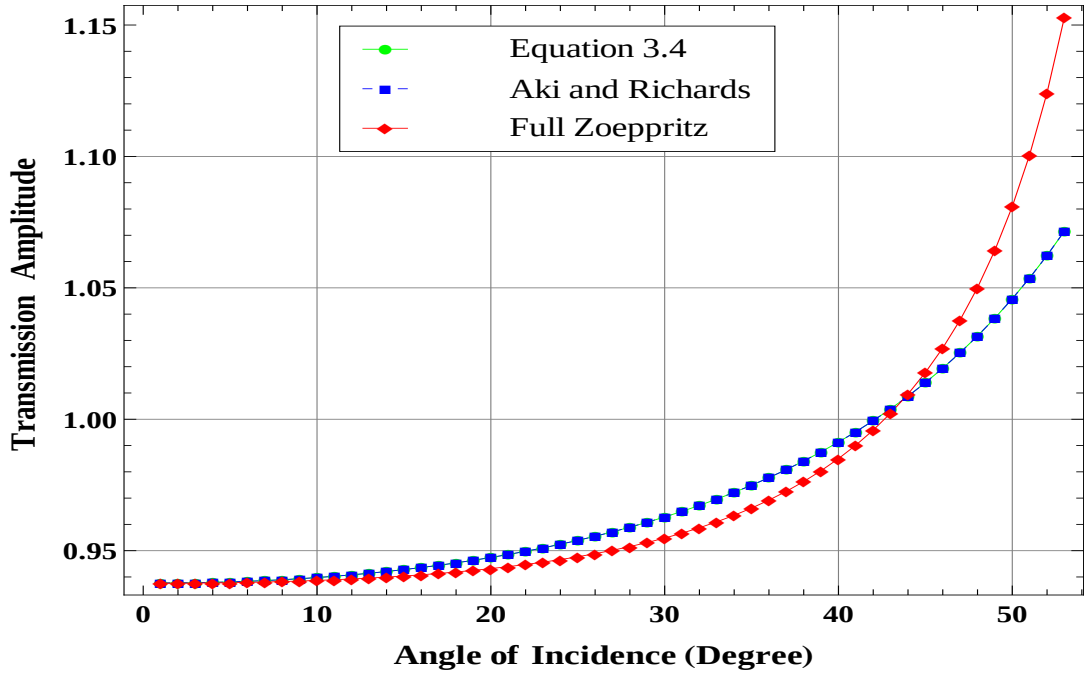

(a) T_{PP} approximation

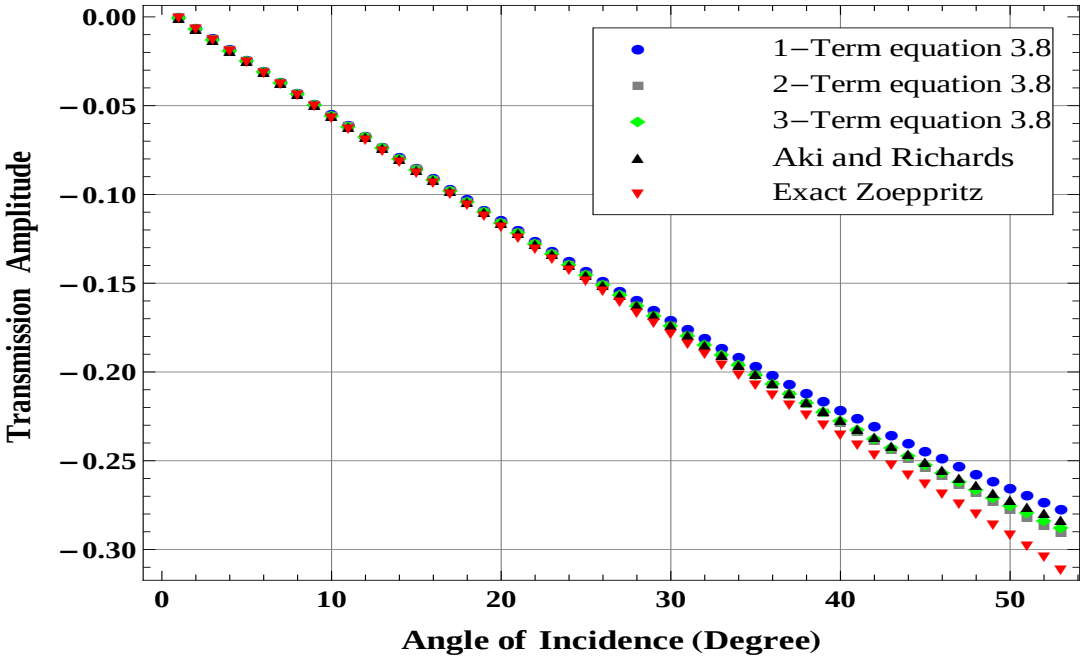

(b) T_{PS} approximation

Figure 3.1: Model 1 approximations for transmission PP and PS coefficients showing responses from Zoeppritz, Aki-Richards and approximations in equation 3.8

$$D = \frac{\beta}{\alpha}\left(\left(\frac{\Delta\beta}{\beta} + \frac{\Delta\rho}{2\rho}\right) - \frac{\beta}{\alpha}\left(\frac{2\Delta\beta}{\beta} + \frac{3\Delta\rho}{4\rho}\right)\right) \tag{3.9b}$$

$$E = \frac{1}{8}\left(\frac{\beta}{\alpha}\left(\frac{2\Delta\beta}{\beta} + \frac{\Delta\rho}{\rho}\right) - \left(\frac{\beta}{\alpha}\right)^4\left(\frac{8\Delta\beta}{\beta} + \frac{5}{2}\frac{\Delta\rho}{\rho}\right)\right) \tag{3.9c}$$

In all of the above expressions, α , β and ρ indicate the average values of P-wave velocity $(\alpha_2 + \alpha_1)/2$, S-wave velocity $(\beta_2 + \beta_1)/2$ and density $(\rho_2 + \rho_1)/2$ across the interface; while $\Delta\alpha = (\alpha_2 - \alpha_1)$, $\Delta\beta = (\beta_2 - \beta_1)$, $\Delta\rho = (\rho_2 - \rho_1)$ indicate the differences in α , β and ρ across the interface and the angle θ is taken as the average between the incidence and transmission angle of the incident P-wave (Shuey, 1985).

Figure 3.1(b) shows a plot of transmission PS amplitude as a function of incidence angle for Zoeppritz, Aki-Richards and my approximations using 1-, 2- and 3-terms with increasing power of $\sin\theta$. From the legend of Figure 3.1(b), 1-term approximation defines a plot of amplitude with offset using only the term with $\sin\theta$ and dropping the higher order terms while 3-terms approximation denotes inclusion of all terms up to $\sin^5\theta$. Similar plots for the other test models are shown in Figures 3.2 and 3.3. The model parameters used to generate the plots are the same for both T_{PP} and T_{PS} and are shown in Table 3.1. Equations 3.5 and 3.9 are the approximations that will be used for the estimation of elastic properties from the T_{PP} and T_{PS} amplitudes.

Table 3.1: Elastic parameters for the test models. Model 1 and 2 are oil- and gas-sand models respectively from Donati and Martins (1998). Model 3 is a gas-sand model from Sheuy (1985)

Model	**Layer 1**			**Layer 2**		
	$\alpha_1(ft/s)$	$\beta_1(ft/s)$	$\rho_1(g/cc)$	$\alpha_2(ft/s)$	$\beta_2(ft/s)$	$\rho_2(g/cc)$
1	10400	5572	2.36	12251	7480	2.27
2	10000	4085	2.40	8005	5348	2.14
3	7569	3091	2.15	6401	4268	1.95

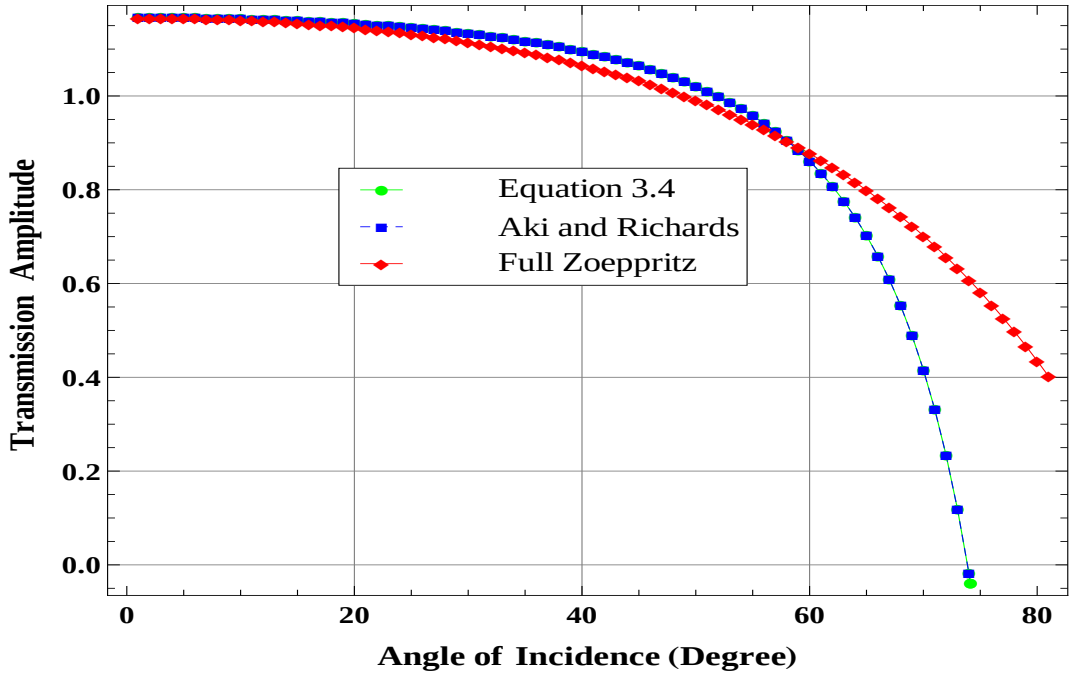

(a) T_{PP} approximation

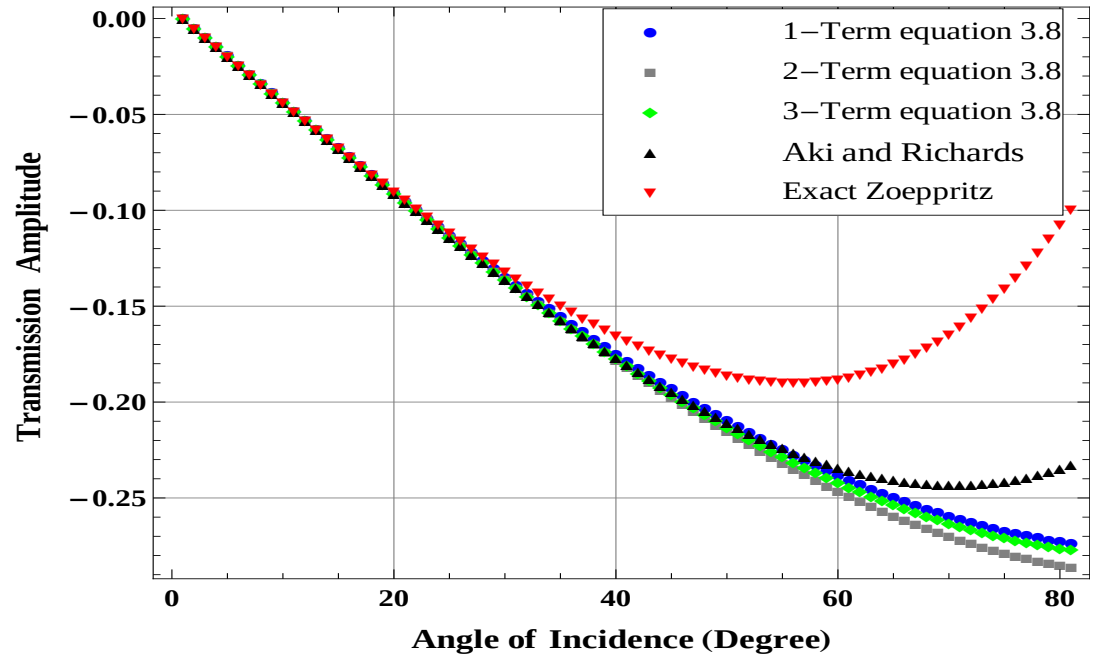

(b) T_{PS} approximation

Figure 3.2: Model 2 approximations for transmission PP and PS coefficients showing responses from Zoeppritz, Aki-Richards and approximations in equation 3.8

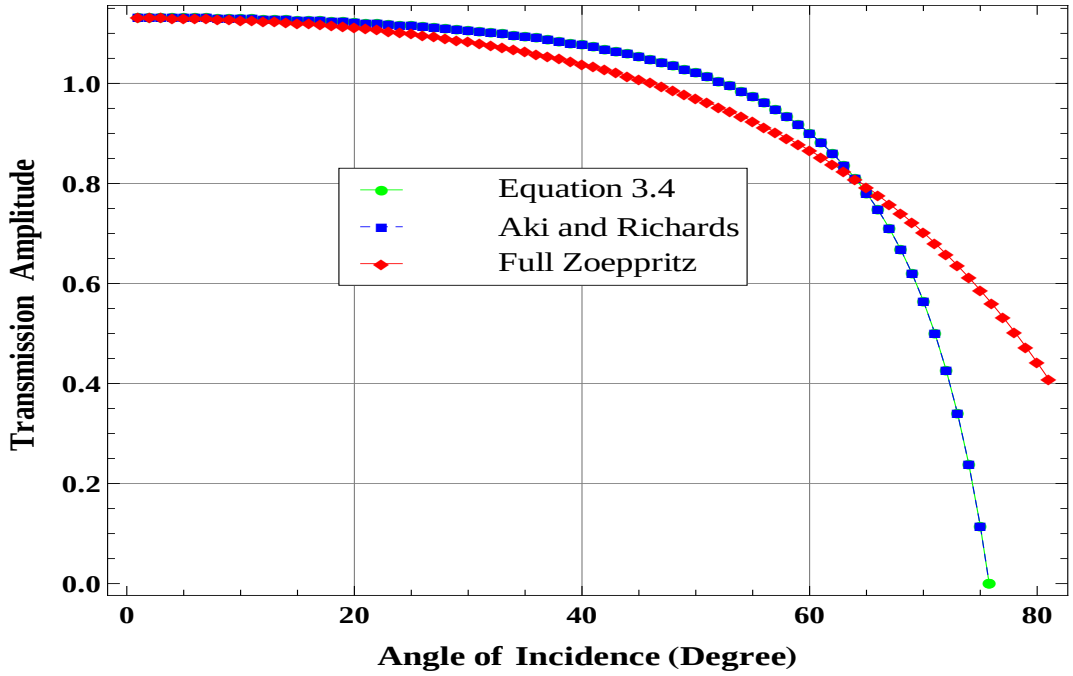

(a) T_{PP} approximation

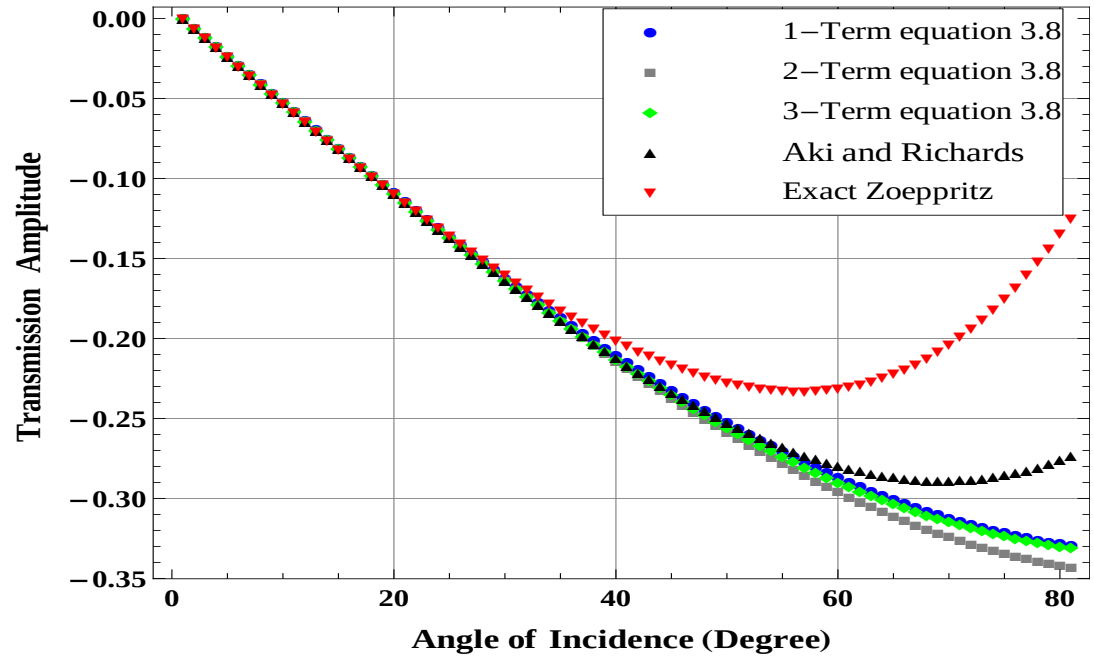

(b) T_{PS} approximation

Figure 3.3: Model 3 approximations for transmission PP and PS coefficients showing responses from Zoeppritz, Aki-Richards and approximations in equation 3.8

3.2 VSP acquisition geometry

VSP data have higher lateral resolution than surface seismic data for the same depth, due to a smaller Fresnel zone. Also, frequencies are higher in VSP data because of their shorter one-way travelpaths through the attenuating near surface and the underlying strata. This yields a wider bandwidth and an improved lateral resolution. Data acquisition in VSP mode consists of a number of receiver levels which are usually at intervals of 66 ft - 82 ft (20 m - 25 m) (Hardage, 2000). The receiver line could be vertical or deviated depending on the trajectory of the borehole involved. A simple vertical borehole trajectory is assumed for this work. In a typical VSP survey, data are usually recorded in common shot gather domain, where a group of traces are recorded by different receivers from the same shot point. For the purpose of this thesis, there is a need to select certain number of receivers out of the whole length of cable. In order to record the transmission amplitudes as a function of incidence angle of the impinging P-wave, receivers that are located beneath the interface of interest are required. A common receiver gather (CRG) is required for the analysis of transmitted amplitudes from each offset that correspond to a particular angle of incidence. A CRG is a group of traces recorded by the same receiver from different shot points. Figure 3.4 shows a typical geometry for a conventional VSP survey. The relationship between offset, which we have control over in terms of inter-shot distances, and the incidence angle of the incoming wave has to be known in order to convert the respective offsets, in a multi-offset/ walkaway-type VSP geometry, into corresponding incidence angles.

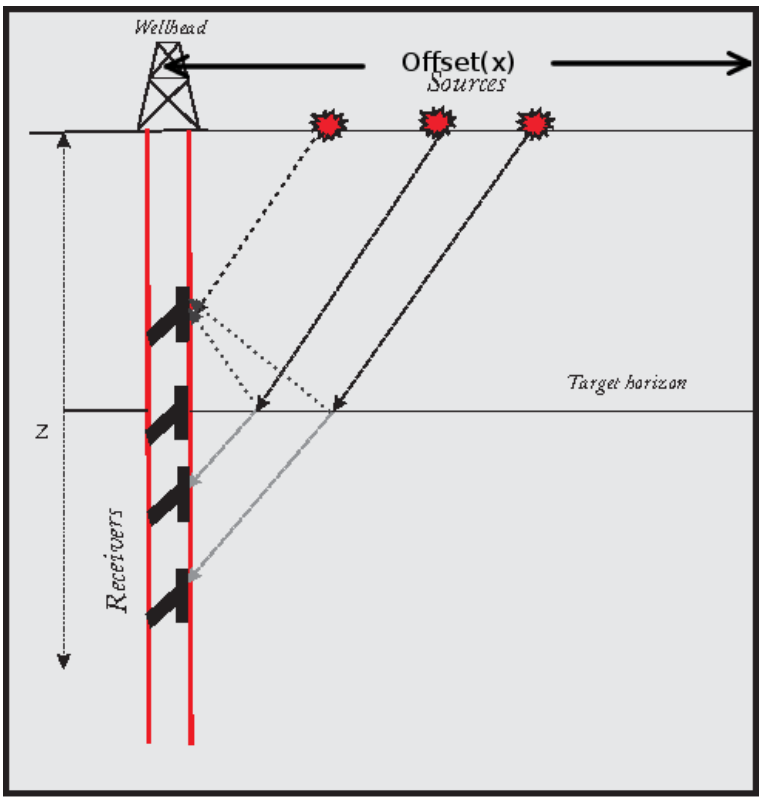

Figure 3.4: Typical VSP acquisition geometry showing shot points on the surface and receivers downhole

3.2.1 Important assumptions

In order to fulfil the set objectives, there are a number of assumptions regarding the physics and geometry of the problem at hand, the method in this work assumes that all models studied are only vertically heterogeneous (no lateral changes in the elastic parameters) and isotropic with no dipping interfaces. The plane wave assumption holds for source - receiver distances that are much longer than the wavelength of the incident wave. This is generally acceptable for pre-critical reflection data at typical exploration frequencies and depths (Castagna and Backus, 1993) and should also hold for transmission events.

The linearized Aki and Richards approximations are made under the assumptions that two solid half-spaces are welded together at an elastic interface, across which there are only small relative changes in elastic parameters, and that the angles involved which is the average P- and S-wave angles of incidence and transmission across the interface are not close to critical angle and generally less than 90° (Aki and Richards, 2002).

Expansion of the T_{PS} equation was made using a Maclaurin's series which is a special type of Taylor's series. This means that the expansion was made around $\theta = 0°$. Therefore, angles of incidence too far from 0° will fail to approximate the starting equation.

3.3 Common receiver gather

In order to obtain the data needed for analysis, the recorded traces have to be sorted into CRGs. Figure 3.5 shows transmitted rays belonging to different CRGs. I obtained a different CRG seismogram each for both T_{PP} and T_{PS} with the assumption that the former is dominant on the Z-component while the latter is dominant on the X-component seismogram respectively.

3.4 Transforming from offset to incidence angle

This is a basic step in AVO analysis because seismic data are often recorded in distance-time *(x,t)* space hence there is a need to transform the offsets *(x)* to corresponding incidence angles θ. If we consider Figure 3.6 consisting a seismic source at the surface and a geophone clamped to the formation downhole. The group of traces obtained in offset domain is termed an offset gather while angle gather is obtained after appropriate transformation into incidence angle (Hampson and Russell, 2004). Assuming straight rays travel path from the shot points (S) to the receivers (R) downhole, the rays strike the interface at an angle θ_1 and is transmitted to the underlying layer with an angle θ_2. From Figure 3.6 below;

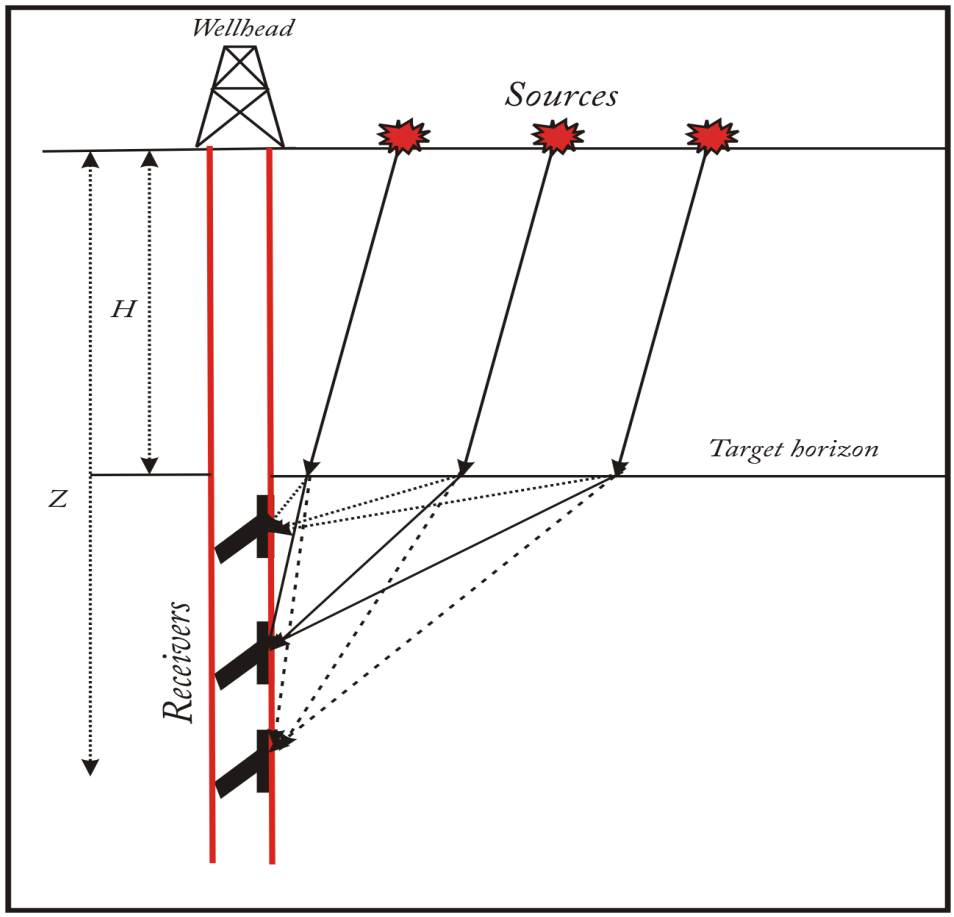

Figure 3.5: Schematic of the concept of CRG sorting of VSP data

$$X1 = (Z - H)\tan(\frac{\pi}{2} - \theta_2), \Rightarrow X1 = (Z - H)\cot\theta_2 \tag{3.10}$$

from snells' law;

$$\sin\theta_2 = \frac{\alpha_2}{\alpha_1}\sin\theta_1 \tag{3.10a}$$

Hence, $\cot\theta_2$ in equation 3.10 becomes;

$$\cot\theta_2 = \frac{\sqrt{1 - \sin^2\theta_2}}{\sin\theta_2}, \Rightarrow \frac{\sqrt{1 - \left(\frac{\alpha_2}{\alpha_1}\right)^2 \sin^2\theta_1}}{\frac{\alpha_2}{\alpha_1}\sin\theta_1} \tag{3.10b}$$

By substituting the above equation into equation 3.10, X1 becomes;

$$X1 = (Z - H)\left[\frac{\sqrt{1 - \left(\frac{\alpha_2}{\alpha_1}\right)^2 \sin^2\theta_1}}{\frac{\alpha_2}{\alpha_1}\sin\theta_1}\right] \tag{3.11}$$

$$X2 = X - X1 = H\tan\theta_1, \Rightarrow X = H\tan\theta_1 + X1 \tag{3.12}$$

If we substitute equation 3.11 into equation 3.12, then we get the relationship between offset X and incidence angle θ as;

$$X = H\tan\theta_1 + (Z - H)\left[\frac{\sqrt{1 - \left(\frac{\alpha_2}{\alpha_1}\right)^2 \sin^2\theta_1}}{\left(\frac{\alpha_2}{\alpha_1}\right)\sin\theta_1}\right] \tag{3.13}$$

It is quite obvious that the relationship between offset and incidence angle in equation 3.13 above is non-linear. There are two possible ways of solving this

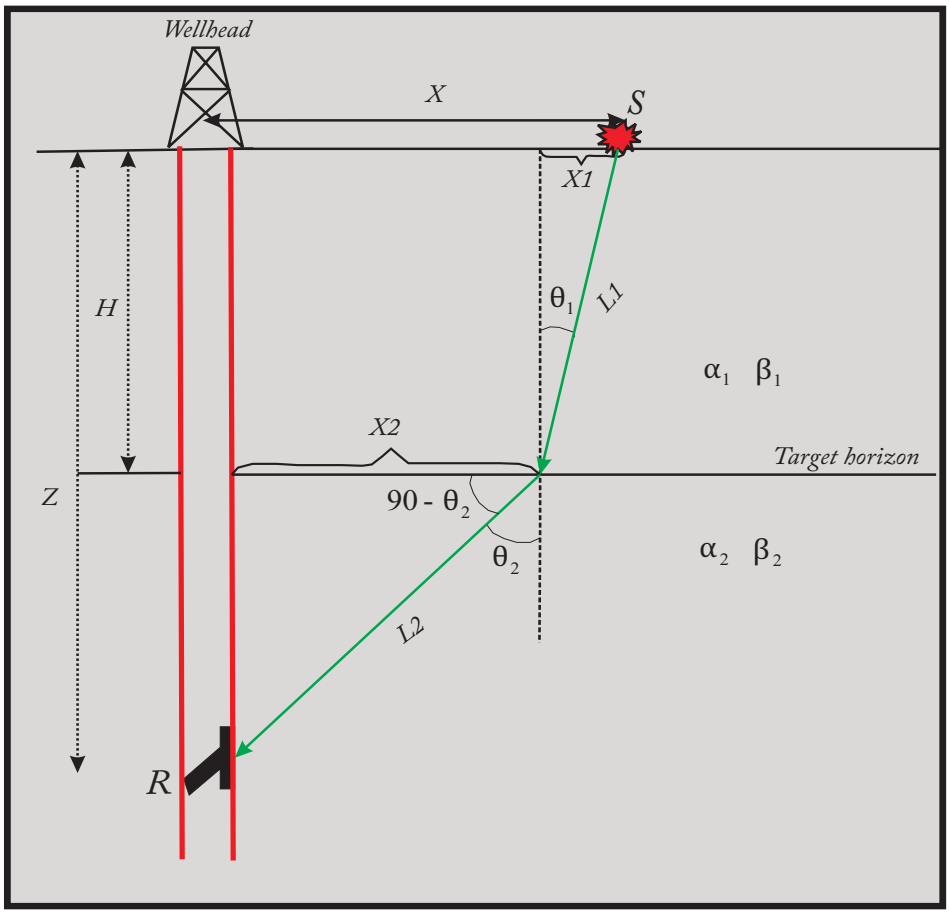

Figure 3.6: Schematic of the geometrical relationship between offset (X) and incidence angle θ_1. H is the depth to the interface of interest and Z is the depth to the receiver of interest. The relationship as shown in equation 3.13 depend on the P-wave velocity of the layer above the interface and the P- and S-wave velocities for the layer below the interface for PP- and PS- angles of incidence respectively

equation namely; (a) numerical method and (b) analytical method. The numerical method entails the use of fixed point or successive approximation methods in which we try to obtain the best value of θ given the values for offset (X), receiver depth (Z), upper layer thickness (H) and P- and S-waves velocity of the upper and lower layers ($\alpha_1, \beta_1, \alpha_2, \beta_2$) respectively. The analytical solution is very complicated and it was only possible with the aid of a Mathematica® program (Appendix B). I chose to use the analytical solution over the numerical solution that is less accurate and even breaks down completely at large offsets.

It is also possible that a theoretical curve be generated for the purpose of this transformation. Figure 3.7 shows the curve of the offset-angle data pair computed from equation 3.12. A quadratic function fitted to this data pair is of the form

$$\theta = Mx + Nx^2 \tag{3.14}$$

where **M** and **N** are constants. The values of these coefficients are very similar for all the test models. The figure also shows a close compliance of the curve for the three models with an extrapolated curve to very far offset computed from the function in equation 3.14. Figure 3.8 shows a closer look at the curves. Therefore, I think such a curves could be used as a quick way to estimate incidence angles from offsets.

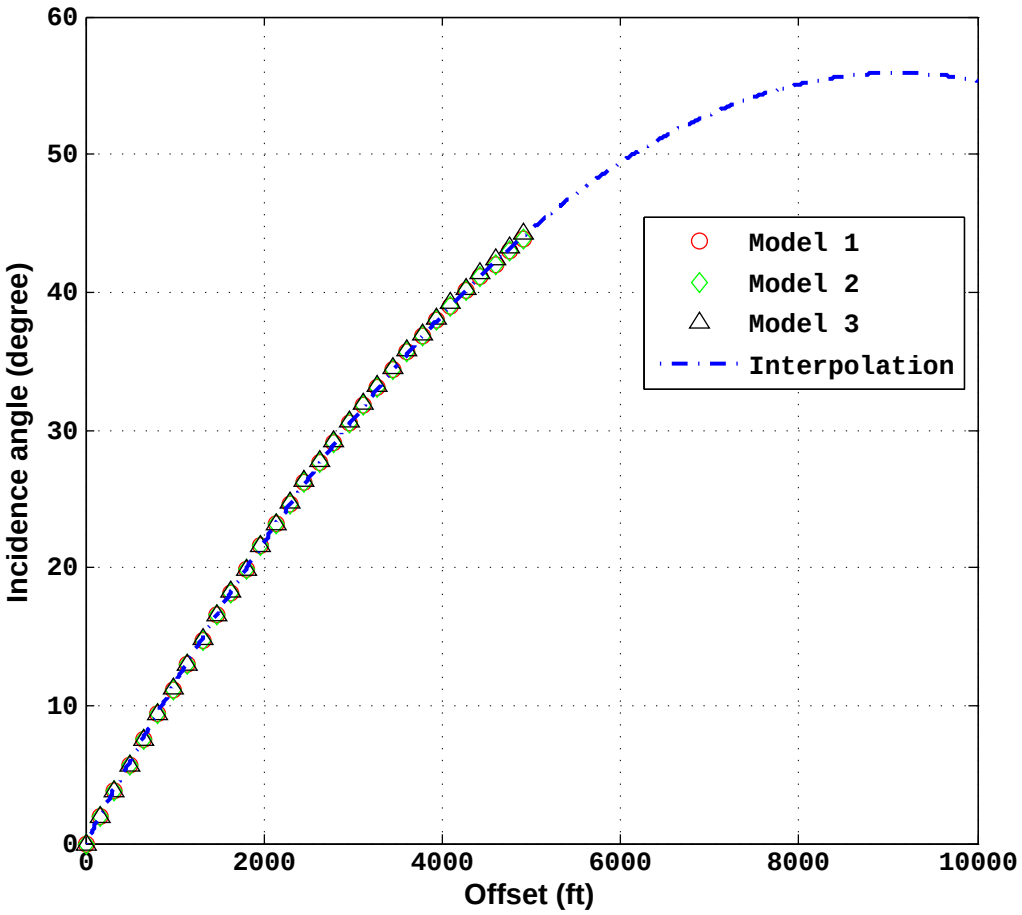

Figure 3.7: Theoretical curves of Model 1, 2 and 3 with an extrapolated curve including far offset. Curve like this can be generated for offset-incidence angle transformation for an area of interest

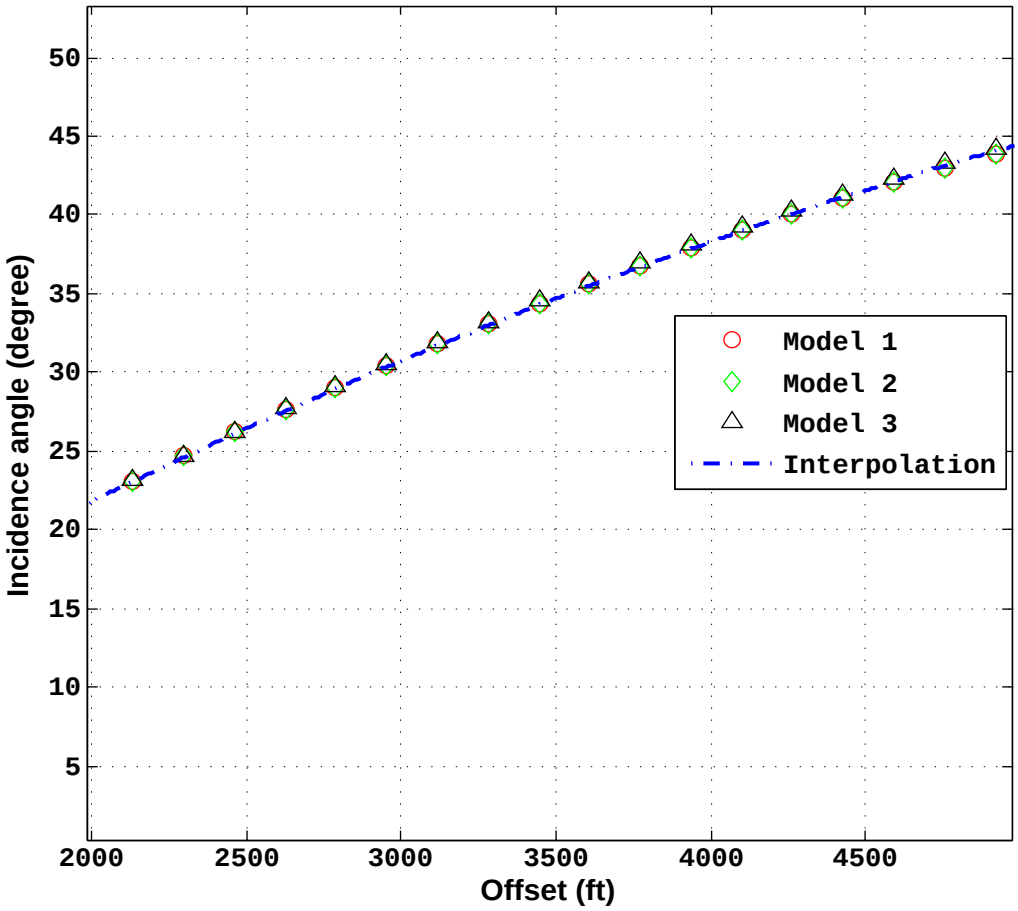

Figure 3.8: A zoomed-in version of Figure 3.7 showing a closer look at the points. The trends of the curves are quite close to one another for all the models and the interpolated curve

CHAPTER 4

SYNTHETIC DATA GENERATION

4.1 Test models description

Three different published reservoir models were used for testing the concepts and methods in this thesis. The first two (Model 1 and 2) are models of an oil and gas-sand respectively underlying a shale layer (Donati and Martin, 1998). Model 3 is also a gas-sand model with elastic parameters typical of the Gulf of Mexico basin (Shuey, 1985). Information about the porosity of these sands are not available from the referenced works for Model 1 and 2, but the sand in Model 3 has 30% porosity (Shuey, 1985). The depth to the top of the sand is assumed to be at 2625ft ($\approx$ 800m). Figures 4.1, 4.2 and 4.3 show the P- and S-wave velocities and densities respectively for the three models. The values of the parameters are also summarized in Table 3.1.

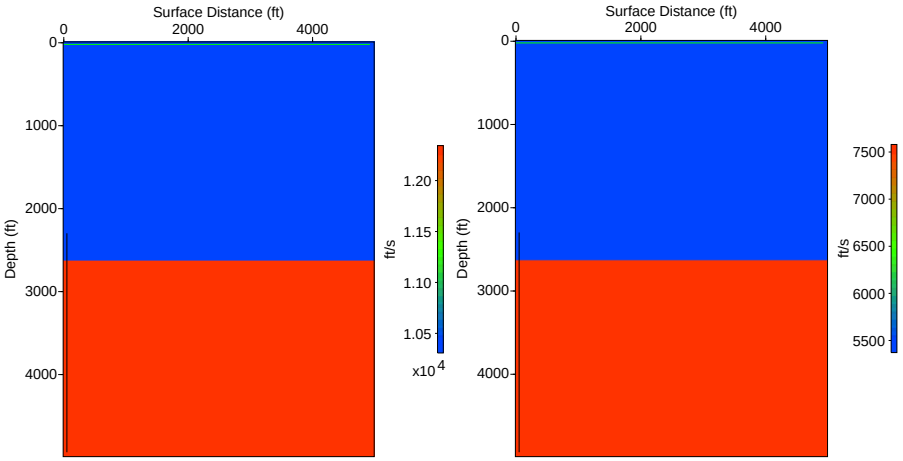

(a) P-wave velocity

(b) S-wave velocity

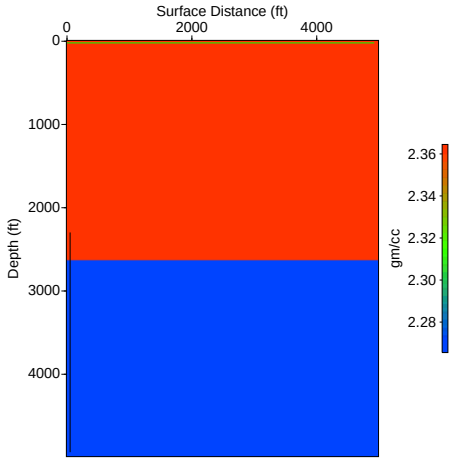

(c) Density

Figure 4.1: Elastic parameters for reservoir Model 1 showing P-wave, S-wave velocity and density in (a), (b) and (c) respectively

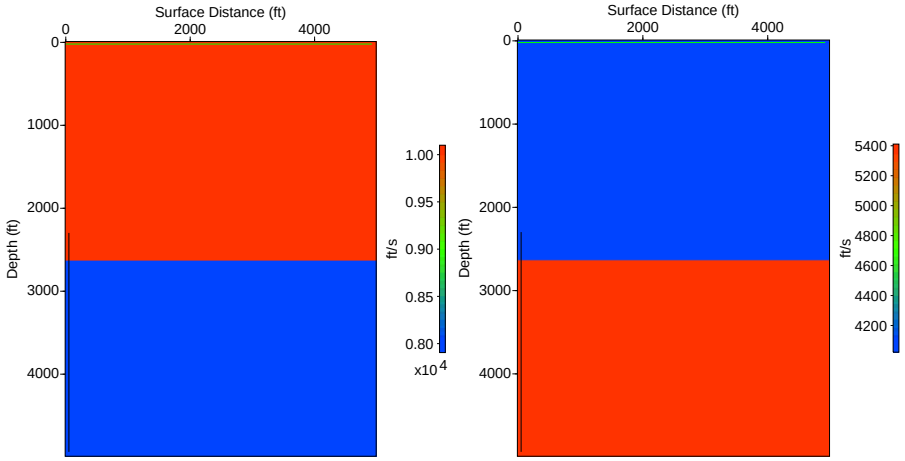

(a) P-wave velocity

(b) S-wave velocity

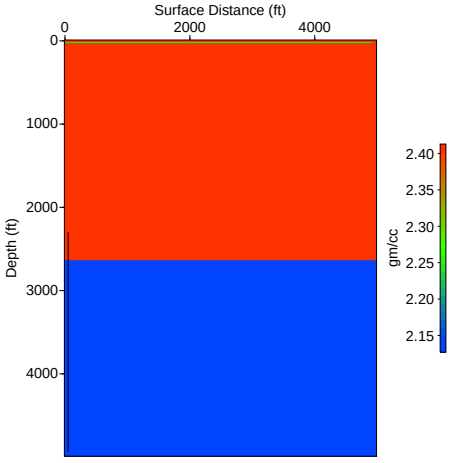

(c) Density

Figure 4.2: Elastic parameters for reservoir Model 2 showing P-wave, S-wave velocity and density in (a), (b) and (c) respectively

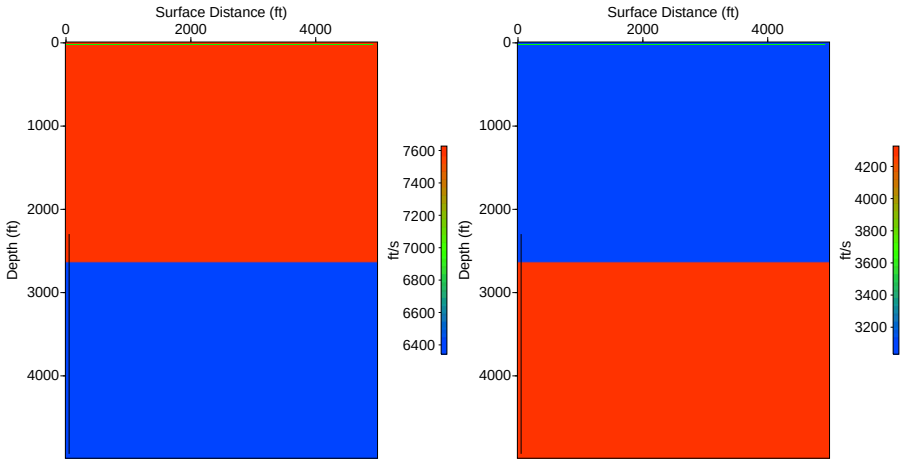

(a) P-wave velocity

(b) S-wave velocity

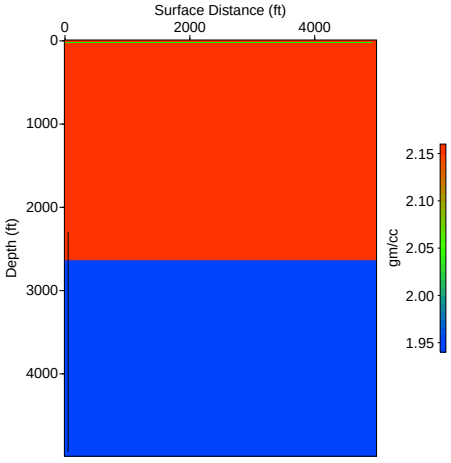

(c) Density

Figure 4.3: Elastic parameters for reservoir Model 3 showing P-wave, S-wave velocity and density in (a), (b) and (c) respectively

4.2 Synthetic data generation

The forward problem entails computing the amplitudes for a given model as a function of the incidence angle, which will later be inverted for elastic parameter contrasts. The scattering matrix as given by Aki and Richards (2002) is shown as follows.

$$S = \begin{pmatrix} \grave{P}\acute{P} & \grave{S}\acute{P} & \acute{P}\acute{P} & \acute{S}\acute{P} \\ \grave{P}\acute{S} & \grave{S}\acute{S} & \acute{P}\acute{S} & \acute{S}\acute{S} \\ \grave{P}\grave{P} & \grave{S}\grave{P} & \acute{P}\grave{P} & \acute{S}\grave{P} \\ \grave{P}\grave{S} & \grave{S}\grave{S} & \acute{P}\grave{S} & \acute{S}\grave{S} \end{pmatrix} \tag{4.1}$$

The equations given by Aki and Richards (2002) are simplification of the entries of this matrix for various media of incidence of P- and S-wave modes. The entry in column 1 row 3 and 4 are expressions for downgoing P- wave to downgoing P-and S-wave respectively.

I used thirty-one shot points in the model that goes from 0 to 4920 ft in a step of 164 ft. As I mentioned earlier, the interface of interest was put at 2625 ft and the geophone that records the amplitudes from each shot was put at a depth of 4937 ft. Because each shot offset is progressively further away from the borehole, rays strike the interface at different angles and are detected at different times. As expected, the time depends on the P-wave velocity of the layer above the interface and also the P- and S-wave velocities of the layer below the interface for the arrivals of T_{PP} and T_{PS} events respectively. The time taken for each of the

events to arrive can be calculated by considering the travel-time from a particular surface shot point to the receiver downhole computed as follows, and depicted in Figure 3.6.

$$L1 = \sqrt{{X_2}^2 + H^2} \tag{4.2}$$

$$L2 = \sqrt{{X_1}^2 + (Z - H)^2} \tag{4.3}$$

therefore, the time taken for the ray to travel from S to R for T_{PP} and T_{PS} respectively are;

$$t_{PP} = \frac{L1}{\alpha_1} + \frac{L2}{\alpha_2} \tag{4.4}$$

$$t_{PS} = \frac{L1}{\alpha_1} + \frac{L2}{\beta_2} \tag{4.5}$$

Figure 4.4 shows a schematic diagram of the modeling setup. The parameters are summarized in Table 4.1. The angle obtained from the transformation of offset to incidence angle is substituted into Aki-Richards (2002) expression for T_{PP} and T_{PS}. The respective amplitude values obtained were assigned to their corresponding travel-times as a series of transmisivity coefficients which is later convolved with a 40-Hz zero-phase ricker wavelet displayed as a CRG of seismic traces as shown in Figure 4.5.

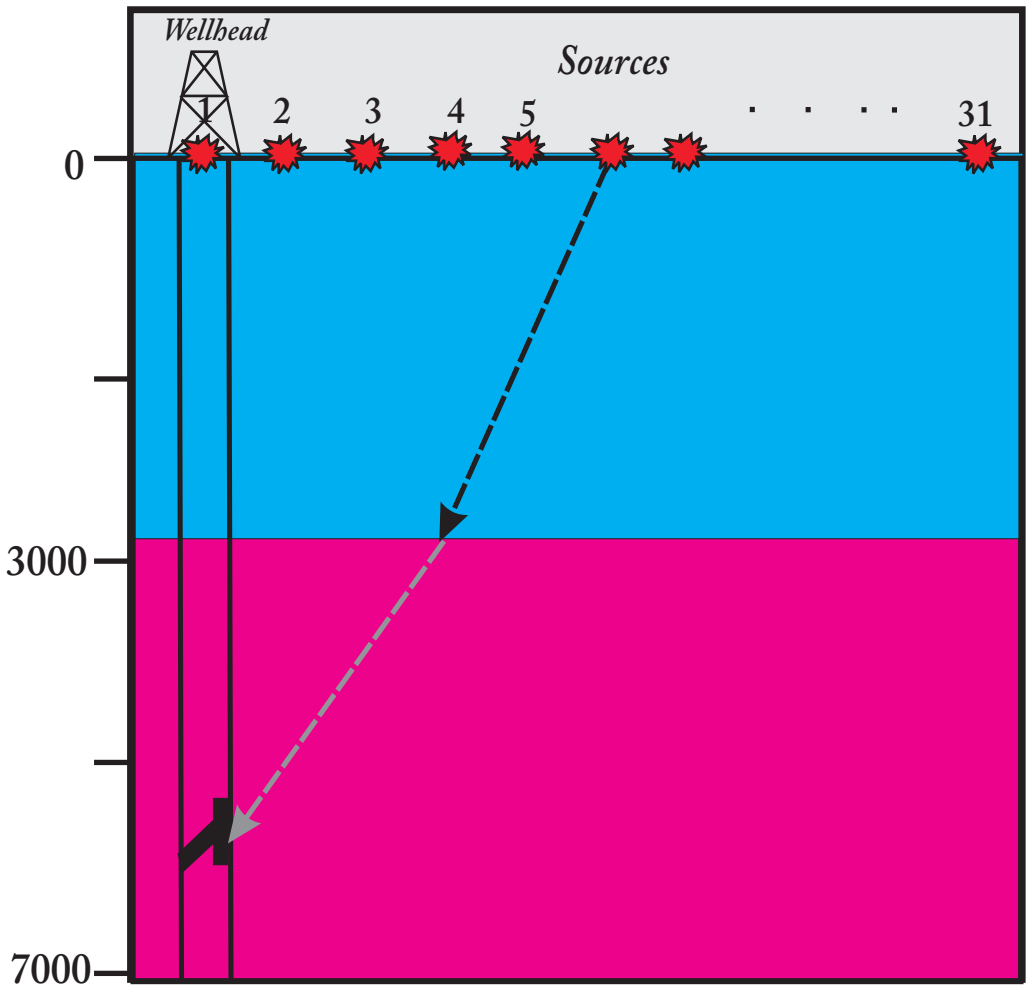

Figure 4.4: Schematic of a walkaway VSP geometry used for forward modeling and generation of a synthetic CRG seismogram

Table 4.1: Forward modeling parameters for synthetic data generation with each parameters and their respective values shown

Parameter	**Value**
Target interface depth (ft)	2625
Source type	Compressional
Wavelet type	zero-phase Ricker
Frequency (Hz)	40
First shot point (ft)	(0,0)
Shot point increment (ft)	164
Number of shots	31
First receiver depth (ft)	2297
Number of receivers	41

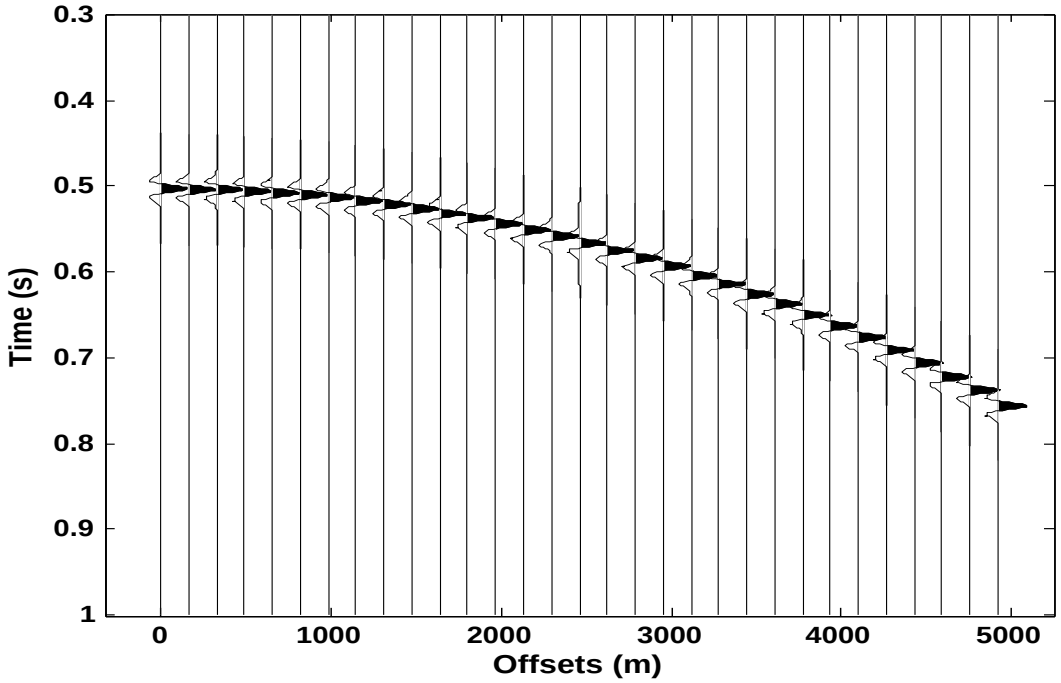

(a)

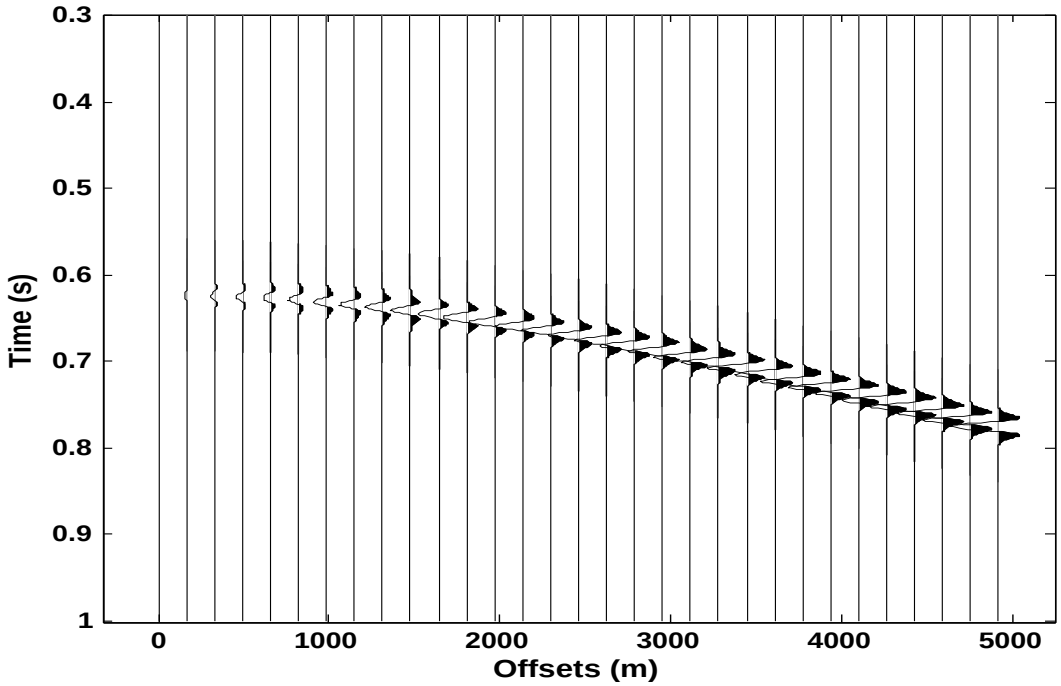

(b)

Figure 4.5: Synthetic CRG for (a) PP-transmission and (b)PS-transmission events for Model 1

CHAPTER 5

RESULTS AND DISCUSSION

5.1 Analysis of transmission coefficients approximations

The plots comparing my approximations for both T_{PP} and T_{PS} with the Aki and Richards (2002) equations are shown in Figures 3.1 - 3.3. In all the models, the range of incidence angles considered are either up to 90% of the critical angle, in cases where it exists, or up to 80° in cases where it does not exist.

Discrepancies between my approximations and the starting Aki and Richards (2002) expressions are described in term of percentages. For all the three models, $T_{PP}(\theta)$ approximations fit well with the Aki and Richards expression within less than 0.001%. However, the same is not the case for $T_{PS}(\theta)$. In model 1, one term approximation is good for the T_{PS} up to 55° which is even more than 90% of the critical angle with error of less than 10%. Likewise, two- and three-term approximations gave errors that are less than 10% up to 50°. Considering

models 2 and 3, there is no critical angle for these two cases and the maximum angle of incidence to considered was 80°. The result of T_{PP} approximation is similar to that obtained for the case of model 1 with error of less than 0.001%. Errors in T_{PS} between the Aki and Richards (2002) and my approximations vary slightly for model 2 and 3. Generally, the error is small at short offset and becomes progressively larger as we move towards large offset. The benchmark at which the incidence angle (θ) conforms with my accuracy standard (i.e., error from Aki and Richards (2002) is less than 10% or incidence angle reaches 90% of the critical angle) for model 2 and 3 is up to 55°. This value is still reasonably good for typical practical exploration cases in which the angle of incidence rarely exceeds 45° (Stewart et al., 2002). There is an error of 4.5% for incidence angle of 45° in model 2 for the 3-term T_{PS} approximation and about 4.0% for model 3. Figures 5.1 and 5.2 show the errors between my approximation for T_{PP} (equation 3.4) and 3-term T_{PS} approximation (equation 3.8) and the Aki and Richards (2002) approximations for T_{PP} and T_{PS} respectively at different angles of incidence. T_{PP} equation shows almost 0% error in the amplitude computed with my expression for T_{PP} and the T_{PP} equation given by Aki and Richards (2002). This is because it was easier to linearize this equation without any further approximation. However, the 3-term T_{PS} equation as given in equation 3.8, agrees very well with the starting Aki and Richards (2002) T_{PS} equation in amplitude values at small to intermediate angles of incidence but the error between the two becomes significant at fairly high incidence angle beyond 60°.

This is due to the approximation in the truncated Maclaurin's series required to linearize the equation as in equation 3.8.

5.2 Elastic parameter change across the interface

The test case models consist of two gas sand and an oil sand overlain by shale. The two gas sand models were obtained from different sources. They, however, showed striking similarities in their responses. Figure 4.1, 4.2 and 4.3 visually depict the elastic parameters. In model 1, both P- ans S-wave velocities increase across the interface by 18% and 37% respectively while there is a reduction in density by 3.8%. In the case of model 2, there is a decrease in P-wave velocity and density across the interface corresponding to 20% and 11% respectively while the S-wave velocity increases by 31%. Model 3 showed a similar trend with 15% and 9% decrease in P-wave and density respectively and a 38% increase in S-wave velocity.

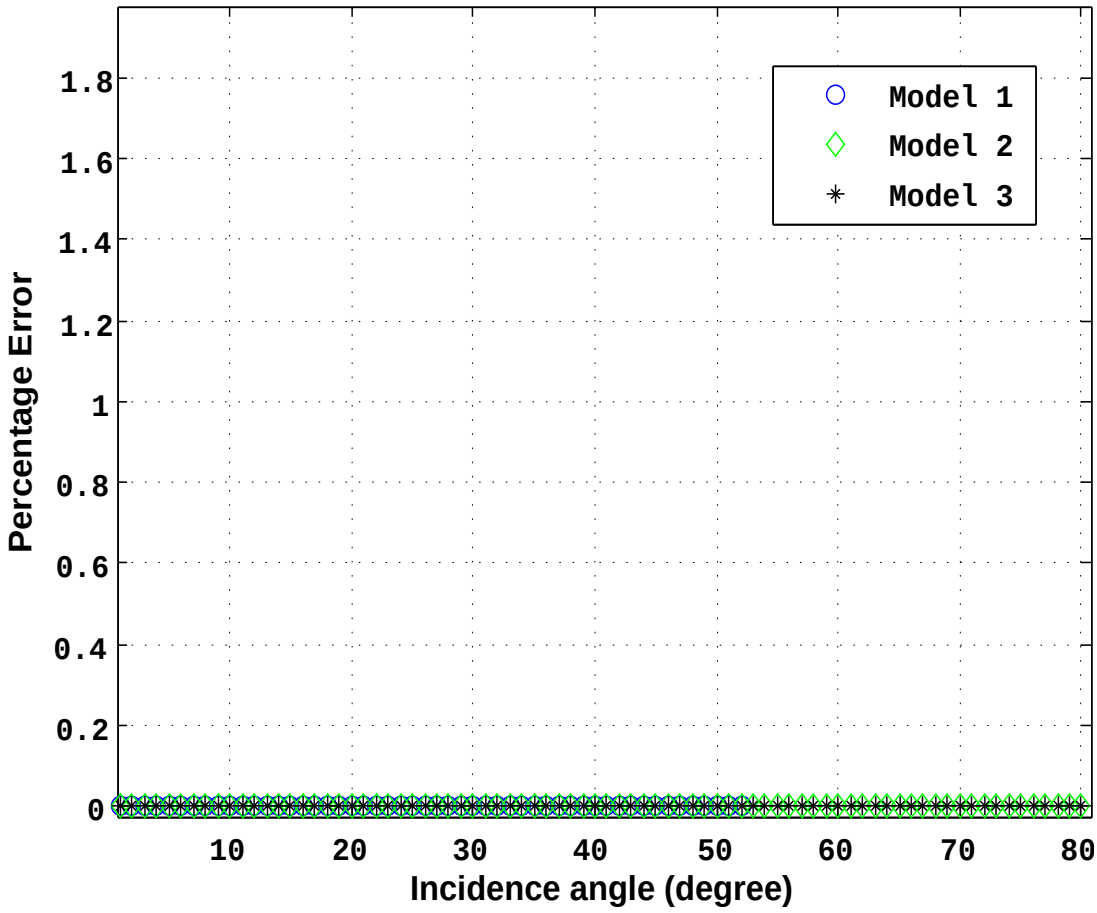

Figure 5.1: Percentage error between equation 3.7 and equation 3.1 for T_{PP}

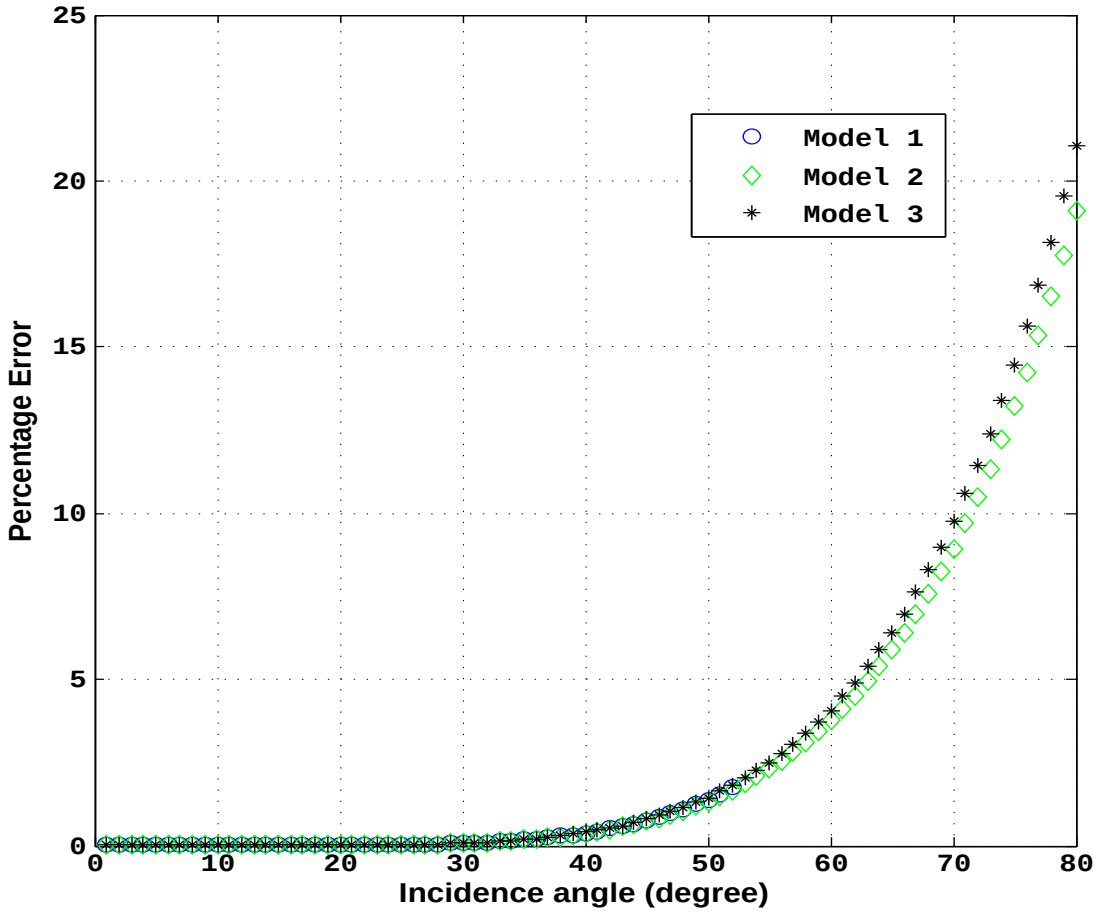

Figure 5.2: Percentage error between equation 3.8 and equation 3.2 for T_{PS}

5.3 Elastic parameters estimation

Using equations 3.5 and 3.9, the elastic parameters of a model could be estimated by least square linear regression analysis on the amplitude vs offset plot. The idea is to estimate three parameters which are β/α, $\Delta\beta/\beta$ and $\Delta\rho/\rho$ from the T_{PS} amplitudes obtained from the synthetic data. Figures 5.3, 5.4, 5.5 show the fit of the function in equation 3.8 to the amplitude versus $\sin\theta$ plot to obtain the coefficients C, D and E for Models 1, 2 and 3 respectively. With this, equations 3.9a, 3.9b and 3.9c can be solved simultaneously for β/α, $\Delta\beta/\beta$ and $\Delta\rho/\rho$, then these values will be compared to the values computed from the exact starting model parameters.

Although, information contained in T_{PP} can be obtained from other sources, such as $\Delta\alpha/\alpha$ from surface seismic, however, it is worth mentioning that the T_{PP} approximation is easier to linearize and does not require further approximation as against T_{PS} which required another approximation in order to linearize it. As a result, T_{PP} amplitude inversion resulted in better estimate of $\Delta\alpha/\alpha$ and $\Delta\rho/\rho$ with the following expressions from equation 3.5:

$$\Delta\alpha/\alpha = 2B \tag{5.1}$$

and

$$\frac{\Delta\rho}{\rho} = 2[1-(A+B)] \tag{5.2}$$

where A and B are the intercept and slope respectively from a straight line fit to the T_{PP} amplitude versus $\tan^2\theta$. Figure 5.6 shows an example of fit to the T_{PP} amplitude for model 2.

The elastic parameter estimates in terms of C, D and E from T_{PS} amplitude curves are algebraically more complicated than the T_{PP} case. The simplest of them is the equation relating β/α and it is given by;

$$\beta/\alpha = \frac{1}{6}\left(\frac{6D}{C} - \frac{(C+6D)^2}{C(K+6\sqrt{6}Q)^{1/3}} - \frac{(K+6\sqrt{6}Q)^{1/3}}{C}\right) \tag{5.3}$$

Where

$$K = C^3 - 108CD^2 - 216D^3 + C^2(-90D + 432E) \tag{5.4}$$

$$Q = \sqrt{-C^2(C - 36(D - 6E))(2CD^2 + 4D^3 + C^2(D - 4E))} \tag{5.5}$$

The expression for the other elastic parameters contrast from T_{PS} amplitude are given in Appendix C.

Table 5.1 shows the elastic parameters contrasts computed from the true model parameters and that estimated from TAVO analysis for each of the models. The estimated values for T_{PS} are those obtained by fitting to an angle of up to 25°.

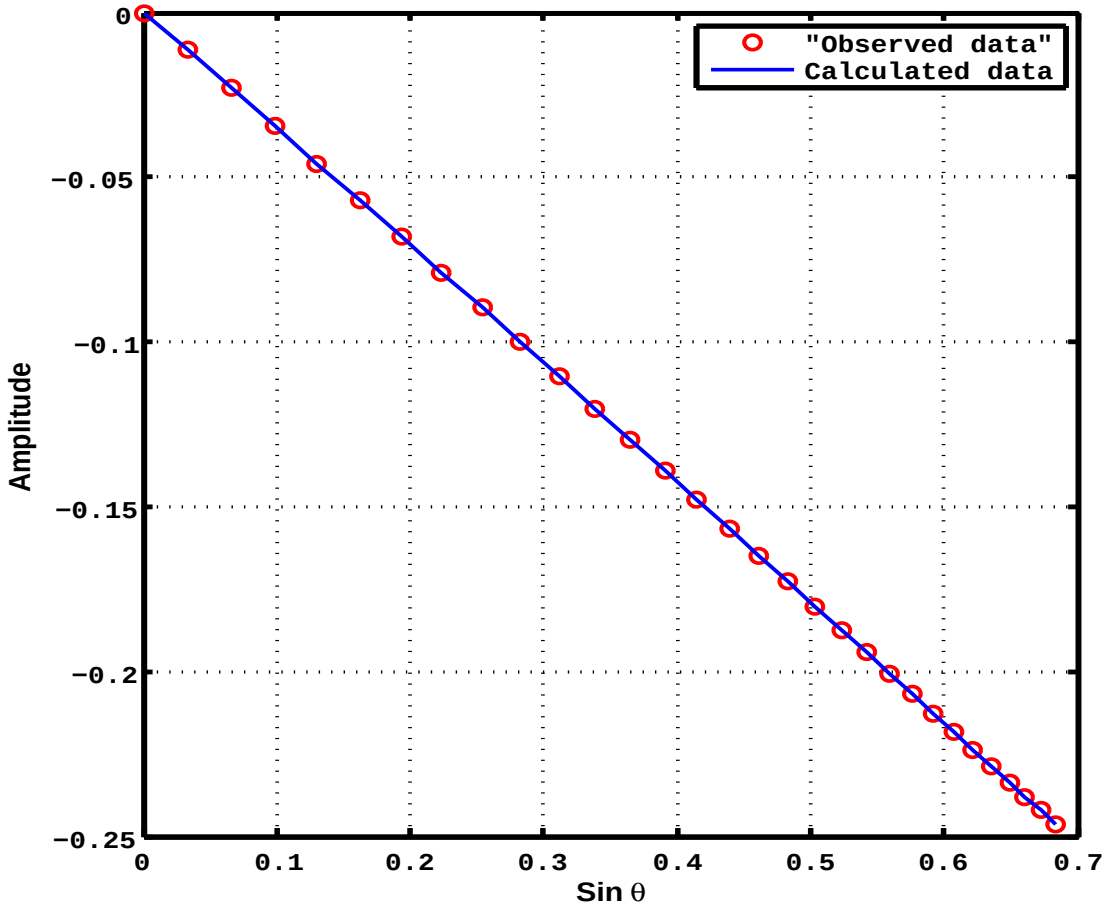

Figure 5.3: Equation 3.9 polynomial function fit to the T_{PS} amplitude of Model 1

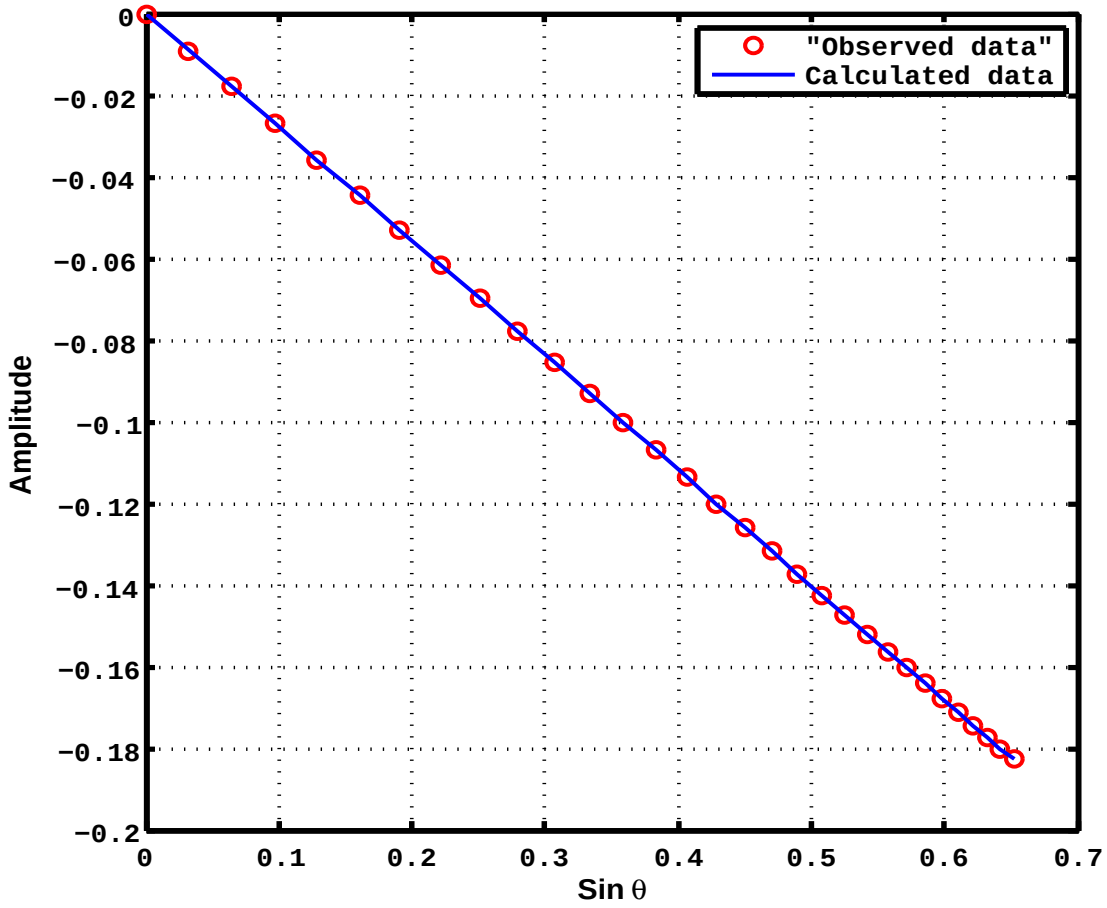

Figure 5.4: Equation 3.9 polynomial function fit to the T_{PS} amplitude of Model 2

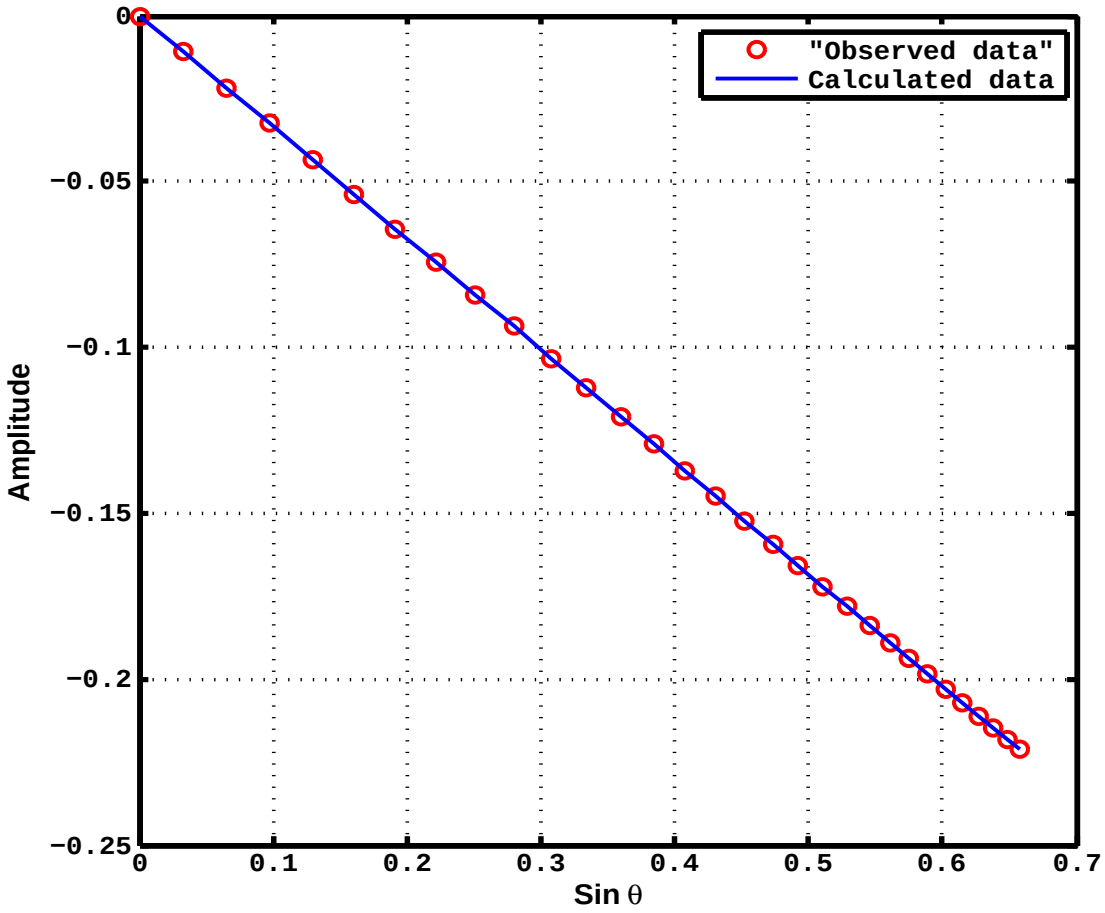

Figure 5.5: Equation 3.9 polynomial function fit to the T_{PS} amplitude of Model 3

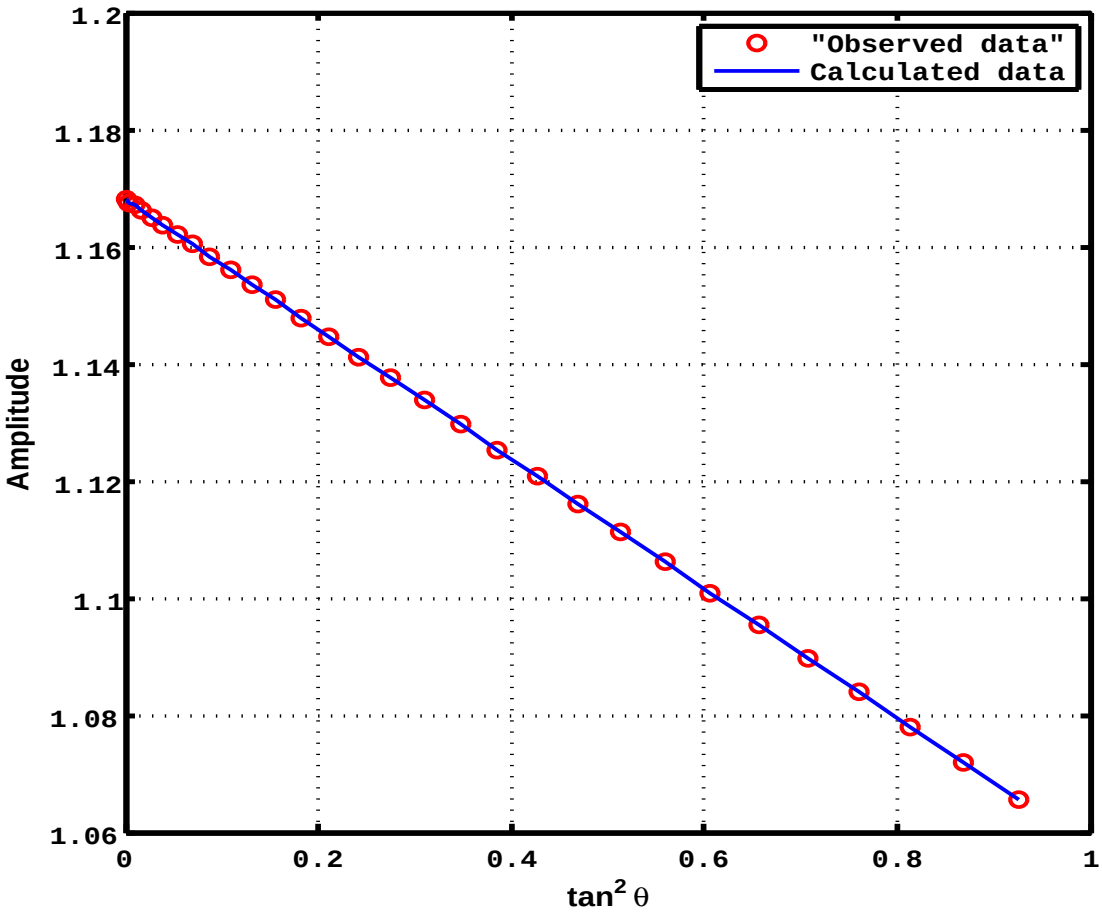

Figure 5.6: Equation 3.5 function fit to T_{PP} amplitude of Model 2

5.4 Accuracy of the regression analysis

Linear regression analysis is an inversion technique, based on least square minimization for estimating model parameters from a given data. Approximation of an equation is bound to have some errors. My approximate functions are fitted to the data generated and the elastic parameters are estimated from it. Because there is a large amount of error in the recovery of the parameters at far offsets especially for $\Delta\rho/\rho$, I successively limit the number of offsets used for the fitting before estimating the contrast in order to reduce the error which generally increases with increasing offset. This procedure is described in the next section in terms of percentage errors for the three parameters inverted from T_{PS} amplitude. In Figure 5.7, 5.8 and 5.9, each point on the x-axis represents the incidence angle corresponding to the furthest offset for each fit. A total of 31 data ponits (offsets/shot points) corresponding to about 45° were initially fitted. It was then reduced to 30 offsets corresponding to about 43° incidence angle and fitted again. This procedure was repeated until 4 offsets corresponding to about 5° was fitted. The purpose of doing this is to study the sensitivity of recovering the elastic parameters at different offset or incidence angle ranges.

Table 5.1: Summary of elastic contrasts estimation from TAVO analysis

		True values from model parameter				Estimated values from TAVO fittings			
	Elastic Parameters	$(\frac{\beta}{\alpha})$	$(\frac{\Delta\rho}{\rho})$	$(\frac{\Delta\beta}{\beta})$	$(\frac{\Delta\alpha}{\alpha})$	$(\frac{\beta}{\alpha})$	$(\frac{\Delta\rho}{\rho})$	$(\frac{\Delta\beta}{\beta})$	$(\frac{\Delta\alpha}{\alpha})$
Model 1	T_{PP}	–	-0.0389	–	0.1634	–	-0.0389	–	0.1634
	T_{PS}	0.5718	-0.0389	0.3101	–	0.6245	0.4597	0.2359	–
Model 2	T_{PP}	–	-0.1145	–	-0.2216	–	-0.1145	–	-0.2216
	T_{PS}	0.5239	-0.1145	0.2678	–	0.5679	0.1163	0.2377	–
Model 3	T_{PP}	–	-0.0976	–	-0.1672	–	-0.0976	–	-0.1672
	T_{PS}	0.5268	-0.0976	0.3199	–	0.5793	0.2629	0.2706	–

5.5 Sensitivity analysis

I present in this sections the limitations of the present study in terms of error analysis and the propagation of these error to the estimation of the elastic parameter contrasts from the T_{PS} amplitude curves.

5.5.1 Error analysis

In this section, I quantify the amount of error associated with the estimation of each of the elastic parameters in section 5.4 for each range of incidence angle used in inversion based on the fittings for all the models. The percentage error between the true parameter contrasts and my estimates of the contrasts for instance error in $\Delta\beta/\beta$ was computed as

$$Percent\ Error\ in\ \frac{\Delta\beta}{\beta} = \left| \frac{\left(\frac{\Delta\beta}{\beta}\right)_{True} - \left(\frac{\Delta\beta}{\beta}\right)_{Estimated}}{\left(\frac{\Delta\beta}{\beta}\right)_{True}} \right| * 100 \qquad (5.6)$$

Figure 5.7 shows the percentage error in β/α. There is an error of less than 10 % up to around 25° incidence angle which progressively increases with offset for the three models in which model 1 is the best and model 3 is worst. Likewise, Figure 5.8, shows the error in the estimation of $\Delta\beta/\beta$ for the three models. It has a similar trend to that in Figure 5.7 with model 2 giving the lowest error at all offsets and model 1 having the highest. In the case of Figure 5.8 depicting error in the estimate of $\Delta\rho/\rho$, the error is very high at all offsets which could probably be due to the higher nonlinearity of the $\Delta\rho/\rho$ equation relative to that of β/α and $\Delta\beta/\beta$ with respect to the estimated linear regression coefficients C, D and E.

5.5.2 Error Propagation analysis

When a quantity, dependent variable, which is a function of one or more different variables with certain amount of error associated with it, is determined, the uncertainties in the independent variable are propagated to the result of the other dependent variable being computed. Therefore, a way to propagate or carry over the uncertainties must be known (Bevington and Robinson, 2003). The estimation of C, D and E from the T_{PS} amplitudes through regression has certain amount of error associated with each of these variables, (i.e., C, D and E) due to the imperfect fit between the model and the data. Therefore, when these regression coefficients are used in the inversion for β/α, $\Delta\rho/\rho$ and $\Delta\beta/\beta$, they contribute to the uncertainty in the estimation of each of the elastic parameter contrasts. The general error propagation formula for any arithmetic operation is given as

$$\delta R = \left|\frac{\partial R}{\partial X}\right| \delta X + \left|\frac{\partial R}{\partial Y}\right| \delta Y + \left|\frac{\partial R}{\partial Z}\right| \delta Z + \dots \tag{5.7}$$

where $R = f(X, Y, Z \dots)$

The quantity $\frac{\partial R}{\partial X}$ for example in equation 5.7 represents the sensitivity with which R reacts to absolute perturbations, δX, in X. It is also called the condition number (Stoer and Bulirsch, 1993). Using similar analysis, the sensitivity of each of the estimated elastic parameter contrasts could be analyzed with respect to the uncertainties in C, D and E as given, for instance, in the case of $\Delta\beta/\beta$.

$$\delta\left(\Delta\beta/\beta\right) = \left|\frac{\partial\left(\Delta\beta/\beta\right)}{\partial C}\right| \delta C + \left|\frac{\partial\left(\Delta\beta/\beta\right)}{\partial D}\right| \delta D + \left|\frac{\partial\left(\Delta\beta/\beta\right)}{\partial E}\right| \delta E \tag{5.8}$$

Where $\Delta\beta/\beta = f(C, D, E)$

The different variables in equation 5.8 are computed as shown in Table 5.2 for the estimations presented in Table 5.1. The partial derivatives of β/α, $\Delta\beta/\beta$ and $\Delta\rho/\rho$ as given in Appendix C are obtained with respect to C, D and E. These derivatives are evaluated at the values of C, D and E estimated from regression. The actual errors δC, δD and δE can be found by subtracting the true values of these variables computed using equations 3.9a - 3.9c from the corresponding values estimated from curve fitting.

The condition numbers are very high in the estimation of $\Delta\rho/\rho$ when compared to the estimation of β/α and $\Delta\beta/\beta$. This means that inversion of $\Delta\rho/\rho$ from the regression coefficients C, D and E is very sensitive to small perturbations in the coefficients and will lead to high amounts of error in the inversion. This explains the reason why the percentage error in $\Delta\rho/\rho$ is high as seen in Figure 5.9. Therefore, in Model 2, for instance, the inverted elastic parameter contrasts from T_{PS} amplitude are 0.5670 ± 0.0418 , 0.2377 ± 0.0211 and 0.1163 ± 0.190 for β/α, $\Delta\beta/\beta$ and $\Delta\rho/\rho$ respectively.

The parameters used to compute the absolute errors associated with each of the elastic parameter contrasts, equation 5.8, is peculiar to the models used in this study and cannot be generalized. A similar analyses have to be carried out for models with different elastic parameters in order to quantify the errors associated with that particular model.

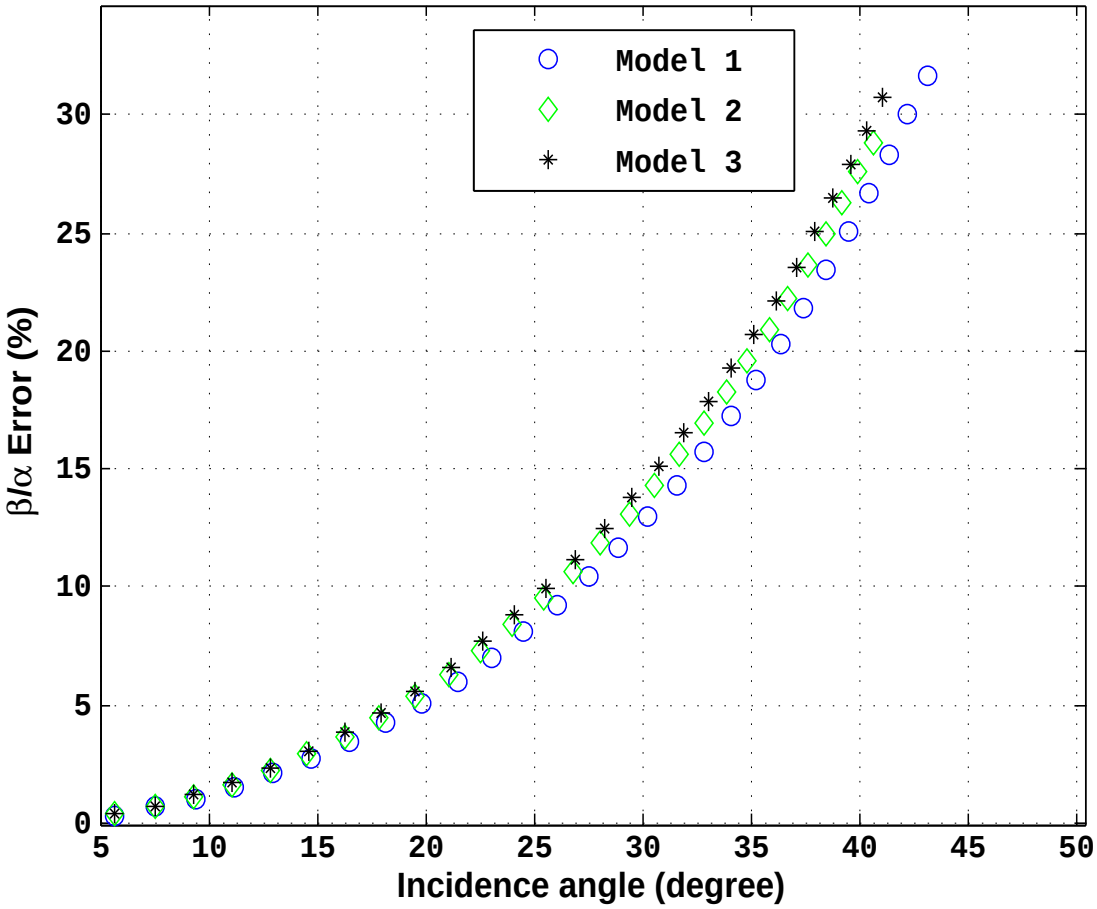

Figure 5.7: Percentage error associated with the estimation of β/α at different range of incidence angle. Model 1 showed the least percent error and model 3 had the most error

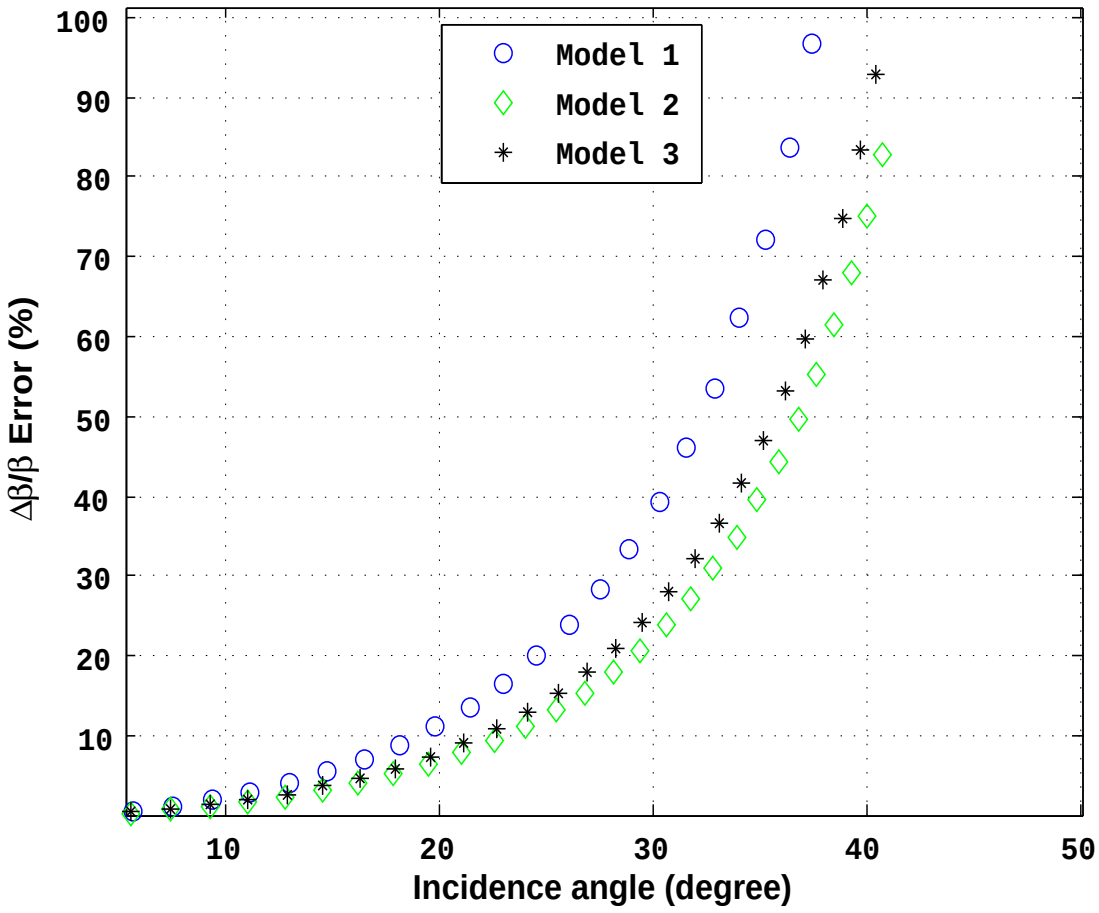

Figure 5.8: Percentage error associated with the estimation of $\Delta\beta/\beta$ at different range of incidence angle. Model 2 showed the least percent error and model 1 had the most error

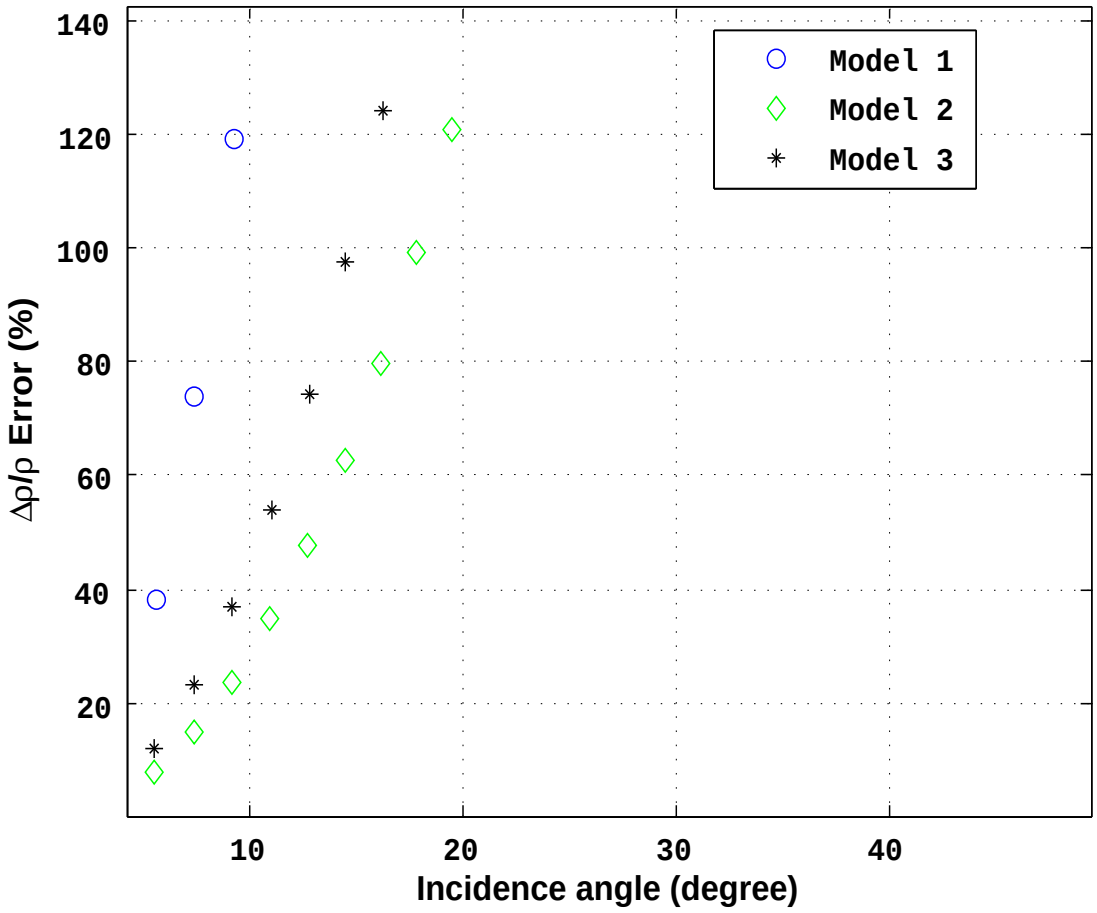

Figure 5.9: Percentage error associated with the estimation of $\Delta\rho/\rho$ at different range of incidence angle. The error is very high in all the models even at small incidence angle

Table 5.2: Sensitivity analysis for error propagation in the estimated elastic parameters contrasts from T_{PS} amplitudes

	Model 1	Model 2	Model 3		Model 1	Model 2	Model 3		Model 1	Model 2	Model 3
$\frac{\partial(\beta/\alpha)}{\partial C}$	0.9	0.9	0.7	$\frac{\partial(\Delta\beta/\beta)}{\partial C}$	1.6	1.4	1.4	$\frac{\partial(\Delta\rho/\rho)}{\partial C}$	5.0	3.6	3.7
$\frac{\partial(\beta/\alpha)}{\partial D}$	7.8	9.4	7.5	$\frac{\partial(\Delta\beta/\beta)}{\partial D}$	6.2	4.3	4.5	$\frac{\partial(\Delta\rho/\rho)}{\partial D}$	36.8	23.7	24.4
$\frac{\partial(\beta/\alpha)}{\partial E}$	10.0	13.0	10.5	$\frac{\partial(\Delta\beta/\beta)}{\partial E}$	9.8	6.6	6.9	$\frac{\partial(\Delta\rho/\rho)}{\partial E}$	75.0	57.7	58.5
δC	-0.000012	-0.000006	-0.000011	δD	0.000528	0.000288	0.000485	δE	-0.0053	-0.003411	-0.005074

CHAPTER 6

CONCLUSIONS AND RECOMMENDATIONS

6.1 Conclusions

I have derived approximations for the transmission amplitude versus offset from the Aki and Richards (2002) approximation of the Zoeppritz equations. The two transmitted wave modes have been linearized in order to make estimation of relative changes in elastic properties from the amplitude easy through linear regression analysis. The range of incidence angles to fit the picked amplitudes has to be carefully computed because it could be a potential source of error in the analysis. In order to achieve this, we propose development of some local theoretical curves as presented in this work for offset-incidence angle transformation.

Estimation of elastic parameter contrasts using linear regression on T_{PS} amplitude is not robust, as it has been shown, and quite sensitive to errors in the

approximation. The parameters β/α and $\Delta\beta/\beta$ were recovered better than $\Delta\rho/\rho$ .The estimate of the former were better than the latter at all range of incidence angles. This could be due to the high nonlinearity of the parameter contrast $\Delta\rho/\rho$ with respect to the regression coefficients C, D and E in the T_{PS} amplitude inversion. Also, there was a large propagation of the errors in estimating C, D and E into $\Delta\rho/\rho$ estimate than the other two parameters. A possible way to reduce these errors in the estimation is to assume a constant value for β/α as it is usually done in reflection AVO studies. The ratio could be obtained from the general empirical relationship between P-wave and S-wave (Castagna et al., 1985) or using full-waveform sonic measurement (Stewart et al., 2002). This would make estimation of the other two parameters from T_{PS} more accurate as it would serve as a constraint to the inversion from the regression coefficients. Estimation of parameters from T_{PP} amplitude fitting was quite good for obtaining $\Delta\alpha/\alpha$ and $\Delta\rho/\rho$ but this means an extra effort is needed in picking amplitudes from the T_{PP} seismic section which could be traded for higher accuracy. Analysis based on receiver gather holds for a homogeneous medium but may not be suitable in case of lateral inhomogeneity and anisotropy. This kind of AVO analysis is only applicable to VSP data as it is presented here.

6.2 Recommendations

This study has presented a case for the use of transmitted wave modes in reservoir characterization. I have also highlighted potential benefits of transmitted waves as

opposed to its reflected counterpart. Therefore, in order to improve this promising method, it is recommended that;

- More modeling studies should be carried out to obtain a representative theoretical curve for offset-angle transformation because this is indispensable in AVO modeling and analysis.
- Other expansion methods should be considered for approximating and linearizing the Zoeppritz equations that will possibly be more accurate up to higher angle of incidence than I have used in this study.
- In order to account for lateral heterogeneity and anisotropy in the subsurface, a common transmission point (CTP) sorting of the data should be developed similar to the CDP concept currently used in reflection AVO.
- The method should be extended to multiple layers model and test with synthetic data generated with a FWM software and also tested on real VSP data.

APPENDIX A

DERIVATIONS OF APPROXIMATED TRANSMISSION AMPLITUDES

The equation for transmitted P-wave (T_{PP}) amplitude (Aki and Richards, 2002) is;

$$T_{PP} = 1 - \frac{1}{2}\frac{\Delta\rho}{\rho} + \left(\frac{1}{2\cos^2\theta} - 1\right)\frac{\Delta\alpha}{\alpha} \tag{A-1}$$

which can be broken down into

$$T_{PP} = 1 - \frac{1}{2}\frac{\Delta\rho}{\rho} + \left(\frac{1}{2\cos^2\theta}\frac{\Delta\alpha}{\alpha} - \frac{\Delta\alpha}{\alpha}\right) \tag{A-2}$$

adding two additional terms $-\frac{\Delta\alpha}{2\alpha}$ and $\frac{\Delta\alpha}{2\alpha}$ to equation A-2, we obtain;

$$T_{PP} = 1 - \frac{1}{2}\frac{\Delta\rho}{\rho} - \frac{\Delta\alpha}{2\alpha} + \left(\frac{1}{2\cos^2\theta}\frac{\Delta\alpha}{\alpha} - \frac{\Delta\alpha}{\alpha} + \frac{\Delta\alpha}{2\alpha}\right) \tag{A-3}$$

The above equation can also be written as;

$$T_{PP} = \left(1 - \frac{1}{2}\frac{\Delta\rho}{\rho} - \frac{\Delta\alpha}{2\alpha}\right) + \frac{\Delta\alpha}{2\alpha}\left(\frac{1}{\cos^2\theta} - 1\right) \tag{A-4}$$

$\left(\frac{1}{\cos^2\theta} - 1\right)$ from equation A-4 can be written using trigonometry identity as follow;

$$\frac{1}{\cos^2\theta} - 1 = \frac{1 - \cos^2\theta}{\cos^2\theta} \Rightarrow \frac{\sin^2\theta}{\cos^2\theta} \Rightarrow \tan^2\theta \tag{A-5}$$

Therefore,

$$T_{PP}(\theta) = \left(1 - \frac{\Delta\rho}{2\rho} - \frac{\Delta\alpha}{2\alpha}\right) + \frac{\Delta\alpha}{2\alpha}\tan^2\theta \tag{A-6}$$

$$T_{PP}(\theta) = A + B\tan^2\theta \tag{A-7}$$

where

$$A = \left(1 - \frac{\Delta\rho}{2\rho} - \frac{\Delta\alpha}{2\alpha}\right)$$

$$B = \frac{\Delta\alpha}{2\alpha}$$

Likewise, the equation for transmitted S-wave (T_{PS}) amplitude is (Aki and Richards, 2002);

$$T_{PS} = \frac{p\alpha}{2\cos\phi}\left[\left(1 - 2\beta^2 p^2 - 2\beta^2 \frac{\cos\theta}{\alpha}\frac{\cos\phi}{\beta}\right)\frac{\Delta\rho}{\rho} - 4\beta^2\left(p^2 + \frac{\cos\theta}{\alpha}\frac{\cos\phi}{\beta}\right)\frac{\Delta\beta}{\beta}\right] \tag{A-8}$$

Using the ray parameter p as shown in the equation

$$p = \frac{\sin\theta}{\alpha} = \frac{\sin\phi}{\beta} \tag{A-9}$$

$p\alpha/2\cos\phi$ from equation A-8 can be written as;

$$\frac{\sin\theta}{2\cos\phi} \Rightarrow \frac{\sin\theta}{2\sqrt{1 - \left(\frac{\beta}{\alpha}\right)^2 \sin^2\theta}} \tag{A-10}$$

From equation A-9, $\sin\phi$ can we written as;

$$\sin\phi = \frac{\beta}{\alpha}\sin\theta \tag{A-11}$$

Using trigonometric identity and equation A-11, $\cos\phi$ can be written as;

$$\cos\phi = \sqrt{1 - \sin^2\phi}, \Rightarrow \sqrt{1 - \left(\frac{\beta}{\alpha}\right)^2 \sin^2\theta} \tag{A-12}$$

and also,

$$\cos\theta = \sqrt{1-\sin^2\theta} \tag{A-13}$$

Then, $\cos\phi$ and $\cos\theta$ from equations A-12 and A-13 respectively and equation A-10 can be substituted into equation A-8 to obtain;

$$T_{PS}(\theta) = \frac{\sin\theta}{2\sqrt{1-\left(\frac{\beta}{\alpha}\right)^2\sin^2\theta}}\left[\left(1-2\left(\frac{\beta}{\alpha}\right)^2\sin^2\theta-2\left(\frac{\beta}{\alpha}\right)\sqrt{1-\left(\frac{\beta}{\alpha}\right)^2\sin^2\theta\left(1-\sin^2\theta\right)}\right)\frac{\Delta\rho}{\rho}\right.$$
$$\left.-4\left(\left(\frac{\beta}{\alpha}\right)^2\sin^2\theta+\left(\frac{\beta}{\alpha}\right)\sqrt{1-\left(\frac{\beta}{\alpha}\right)^2\sin^2\theta\left(1-\sin^2\theta\right)}\right)\frac{\Delta\beta}{\beta}\right] \tag{A-14}$$

Equation A-8 is expanded by Maclaurin's series expansion in terms of $\sin\theta$ and simplified to obtain;

$$T_{PS}(\theta) \approx \left(\frac{-2\Delta\beta}{\alpha}+\frac{\Delta\rho}{2\rho}-\frac{\beta\Delta\rho}{\alpha\rho}\right)\sin\theta+\frac{1}{4}\left(\frac{4\Delta\beta}{\alpha}-\frac{8\beta\Delta\beta}{\alpha^2}+\frac{2\beta\Delta\rho}{\alpha\rho}-\frac{3\beta^2\Delta\rho}{\alpha^2\rho}\right)\sin^3\theta$$
$$+\left(-\frac{\beta^4\Delta\rho}{8\alpha^4\rho}-\frac{\beta^3\Delta\beta}{\alpha^4}\right)\sin^5\theta+\frac{1}{32}\left(\frac{4\Delta\beta}{\alpha}-\frac{24\beta^5\Delta\beta}{\alpha^6}+\frac{2\beta\Delta\rho}{\alpha\rho}-\frac{7\beta^6\Delta\rho}{\alpha^6\rho}\right)\sin^7\theta+\ldots \tag{A-15}$$

This algebra was done with the aid of MATHEMATICA 8.0.

Equation A-15 is truncated at the third term i.e at $\sin^5\theta$ and that is what I have used for the T_{PP}

$$T_{PS}(\theta) \approx \left(\frac{-2\Delta\beta}{\alpha}+\frac{\Delta\rho}{2\rho}-\frac{\beta\Delta\rho}{\alpha\rho}\right)\sin\theta+\frac{\beta}{\alpha}\left(\left(\frac{\Delta\beta}{\beta}+\frac{\Delta\rho}{2\rho}\right)-\frac{\beta}{\alpha}\left(\frac{2\Delta\beta}{\beta}+\frac{3\Delta\rho}{4\rho}\right)\right)\sin^3\theta$$
$$+\frac{1}{8}\left(\frac{\beta}{\alpha}\left(\frac{2\Delta\beta}{\beta}+\frac{\Delta\rho}{\rho}\right)-\left(\frac{\beta}{\alpha}\right)^4\left(\frac{8\Delta\beta}{\beta}+\frac{5}{2}\frac{\Delta\rho}{\rho}\right)\right)\sin^5+\ldots \tag{A-16}$$

Therefore, the expression in equation A-13 can be written in AVO convenient form as;

$$T_{PS}(\theta) \approx C \sin\theta + D \sin^3\theta + E \sin^5\theta \tag{A-17}$$

where

$$C = \left(\frac{-2\Delta\beta}{\alpha} + \frac{\Delta\rho}{2\rho} - \frac{\beta\Delta\rho}{\alpha\rho}\right)$$

$$D = \frac{\beta}{\alpha}\left(\left(\frac{\Delta\beta}{\beta} + \frac{\Delta\rho}{2\rho}\right) - \frac{\beta}{\alpha}\left(\frac{2\Delta\beta}{\beta} + \frac{3\Delta\rho}{4\rho}\right)\right)$$

$$E = \frac{1}{8}\left(\frac{\beta}{\alpha}\left(\frac{2\Delta\beta}{\beta} + \frac{\Delta\rho}{\rho}\right) - \left(\frac{\beta}{\alpha}\right)^4\left(\frac{8\Delta\beta}{\beta} + \frac{5}{2}\frac{\Delta\rho}{\rho}\right)\right)$$

APPENDIX B

OFFSET-ANGLE TRANSFORMATION

MATHEMATICA 8.0 CODE

In[1]:=
```
(*================================================================================*)

(*#*)
(*ENTER VALUES For H,Z,V1,V2 BY MODIFYING THE FOLLOWING FOR A DESIRED MODEL*)
(*#*)
(*        H = Depth of the interface
          Z = Depth of the Receiver recording the Transmission Amplitude,
          Z > H is a neccessary condition   1st receiver=2297*)
(*================================================================================*)

           H = 2625;                        Z = 4937;
(* To compute Tpp(θ) Put V2=P-wave velocity of layer 2*)
(* To compute Tps(θ) Put V2=S-wave velocity of layer 2*)

           Vp1 = 10 000;             Vp2 = 8005;
          Vs1 = 4085;              Vs2 = 5348;

OffsetBegin = 0;          OffsetEnd = 4920;          OffsetStep = 164;
(*================================================================================*)

(*================================================================================*)

(*================================================================================*)

(*#*)
(*DO NOT MODIFY ANY LINE BELOW, GO TO THE SECTION TITLED OUTPUT TO SEE THE RESULTS*)
(*#*)
(*================================================================================*)
```

In[5]:=
```
Syp = Solve[H y * Sqrt[Vp1^2 - Vp2^2 y^2] + Vp2 y (-H + Z) * Sqrt[1 - y^2] == sx * Sqrt[1 - y^2] * Sqrt[Vp1^2 - Vp2^2 y^2], y];
(*Solve the T_PP(θ) or T_PS(θ) case*)
Sys =
  Solve[H y * Sqrt[Vp1^2 - Vs2^2 y^2] + Vs2 y (-H + Z) * Sqrt[1 - y^2] == sx * Sqrt[1 - y^2] * Sqrt[Vp1^2 - Vs2^2 y^2], y];
pNSypositive = Chop[N[Table[pSypositive = Syp[[2]],
     {sx, OffsetBegin, OffsetEnd, OffsetStep}]]];
sNSypositive = Chop[N[Table[sSypositive = Sys[[2]],
     {sx, OffsetBegin, OffsetEnd, OffsetStep}]]];
```

In[9]:=
```
pNTPi = Table[ArcSin[pNSypositive[[i, 1, 2]]], {i, Length[pNSypositive]}];
sNTPi = Table[ArcSin[sNSypositive[[i, 1, 2]]], {i, Length[sNSypositive]}];
```

In[11]:=
```
NPpi = 180 / Pi * pNTPi;
NPsi = 180 / Pi * sNTPi;
```

In[13]:=
```
NTPt = 180 / Pi * (ArcSin[(Vp2 / Vp1) * N[Sin[pNTPi]]]);
NTSt = 180 / Pi * (ArcSin[(Vs2 / Vp1) * N[Sin[sNTPi]]]);
```

In[15]:=
```
aNTPP = (NPpi + NTPt) / 2.0;(*Corresponding theta1 in degrees
  which is an average between reflected and trasnsmitted P-wave angle*)
aNTPS = (NPsi + NTSt) / 2.0 ; (*Corresponding theta1 in degrees which is an
  average between reflected/incident P and trasnsmitted S-wave angle*)
(*where aNTPP is the angle of incident,
Since its only P-wave that is incident from above*)
```

In[17]:=
```
OffsetAngOrig =
  Partition[Riffle[Table[ofst, {ofst, OffsetBegin, OffsetEnd, OffsetStep}], aNTPP], 2];
togeAvePpPs = Table[Append[OffsetAngOrig[[i]], aNTPS[[i]]], {i, 1, Length[aNTPS]}];
ofstPpi =
  Partition[Riffle[Table[ofst, {ofst, OffsetBegin, OffsetEnd, OffsetStep}], NPpi], 2];
ofstPpiPsi = Table[Append[ofstPpi[[i]], NPsi[[i]]], {i, 1, Length[NPsi]}];
aTppTps = Partition[Riffle[NTPt, NTSt], 2];
OffsetAngOrigwPt = Table[Append[OffsetAngOrig[[i]], NTPt[[i]]], {i, 1, Length[NTPt]}];
OffsetAngOrigwPtnSt =
  Table[Append[OffsetAngOrigwPt[[j]], NTSt[[j]]], {j, 1, Length[NTSt]}];
```

```
(*Export the offset and the corresponding
     computed incidence angle for PP and PS transmitted wave-modes &
  the transmission angle of the two wave-modes mentioned above *)

Export["PureInc-PP-PSM2.dat", ofstPpiPsi];
Export["off-Inc-angM2.dat", togeAvePpPs];
Export["M2-trans-PP-PS.dat", aTppTps];
```

In[24]:=
```
DataPairP =
  Partition[Riffle[Table[ofst, {ofst, OffsetBegin, OffsetEnd, OffsetStep}], aNTPP], 2];
(*NTPt is the Transmtd angle only,while NTPP is the average between the
 reflected and transmitted according to AKI and RICHARDS Assumption *)
togeP = Table[Append[DataPairP[[i]], NTPt[[i]]], {i, 1, Length[NTPt]}];
```

In[26]:=
```
DataPairS =
  Partition[Riffle[Table[ofst, {ofst, OffsetBegin, OffsetEnd, OffsetStep}], aNTPP], 2];
togeS = Table[Append[DataPairS[[i]], NTSt[[i]]], {i, 1, Length[NTSt]}];
```

In[35]:=
```
ParaModelFit = Fit[DataPairP, {x^2, x}, x];
CubicModelFit = Fit[DataPairP, {x, x^2, x^3}, x]; (*For PP-Transmission*)
(*ParaModelFit=Fit[DataPairS,{x^2,x,1},x];
CubicModelFit=Fit[DataPairS,{1,x,x^2,x^3},x];*) (*For PS-Transmission*)
```

In[36]:=
```
FitPlot = Show[ListPlot[DataPairP, PlotStyle → Red], Plot[{ParaModelFit, CubicModelFit},
    {x, OffsetBegin, OffsetEnd}, PlotStyle → {Green, Blue}], Frame → True,
   FrameLabel → {"Offset", "Angle of Incidence"}, GridLines → Automatic];
```

In[37]:=
```
FitTest = If [OffsetEnd >= 3280, ParaModelFit, CubicModelFit];
```

In[38]:=
```
FitResult = Style[StringForm["The Relationship is:  θ =  ``", FitTest], FontSize → 14];
DataTable = Style[Grid[Prepend[DataPairP, {"Offset", "Incidence Angle"}],
    Dividers → {{Black, {Black}, Black}}, Frame → True], FontSize → 14];

(*=============================================================================*)

(*                              OUTPUT                                         *)

(* UnComment FitPlot to Visualize the Fitting
 (Note: x==Offset Value              *)
(*=============================================================================*)
```

```
Export["offsetAng-Trans-PPnPS-M2.dat", OffsetAngOrigwPtnSt];
Export["offsetAng-Trans-PP-M2.dat", togeP];
Export["offsetAng-Trans-PS-M2.dat", togeS];
```

In[40]:=
```
FitResult
DataTable
(*FitPlot*)
```

Out[40]= The Relationship is: $\Theta = 0.0122695\,x - 6.73194 \times 10^{-7}\,x^2$

Out[41]=

Offset	Incidence Angle
0	0.
164	1.88928
328	3.77423
492	5.65056
656	7.5141
820	9.36084
984	11.187
1148	12.9889
1312	14.7634
1476	16.5074
1640	18.2183
1804	19.8937
1968	21.5316
2132	23.1302
2296	24.6883
2460	26.2046
2624	27.6785
2788	29.1093
2952	30.4968
3116	31.8409
3280	33.1417
3444	34.3995
3608	35.6148
3772	36.7881
3936	37.9201
4100	39.0116
4264	40.0635
4428	41.0767
4592	42.0522
4756	42.991
4920	43.8941

APPENDIX C

EXPRESSIONS FOR THE ELASTIC PARAMETERS INVERSION FROM TRANSMISSION P-S AMPLITUDE

$$\frac{\beta}{\alpha} = \frac{1}{6}\left(-1 + \frac{6\,D}{C} - \frac{(C+6\,D)^2}{C\,S} - \frac{S}{C}\right)$$

where

$$K = C^3 - 108\,C\,D^2 - 216\,D^3 + C^2\,(-90\,D + 432\,E),$$

$$Q = \sqrt{-C^2\,(C - 36\,(D - 6\,E))\,\left(2\,C\,D^2 + 4\,D^3 + C^2\,(D - 4\,E)\right)} \quad \text{and} \quad S = \left(K + 6\sqrt{6}\,Q\right)^{1/3}$$

$$\frac{\Delta\rho}{\rho} = \frac{2}{9\,(3\,C - 12\,D + 8\,E)^2}\,\left(81\,C^3 - 576\,C^2\,D + 468\,C\,D^2 + 1584\,D^3 + 792\,C^2\,E - 2592\,C\,D\,E + 864\,D^2\,E - 144\,C\,D^2\,L + 288\,D^3\,L + 96\,C^2\,E\,L - 192\,C\,D\,E\,L - C^3\,M^2 + 4\,C^2\,D\,M^2 - 16\,C\,D^2\,M^2 + 8\,C^2\,E\,M^2\right)$$

where

$$P = C^3 - 108\,C\,D^2 - 216\,D^3 + C^2\,(-90\,D + 432\,E),$$

$$R = \sqrt{-C^2\,(C - 36\,(D - 6\,E))\,\left(2\,C\,D^2 + 4\,D^3 + C^2\,(D - 4\,E)\right)},$$

$$L = -1 + \frac{6\,D}{C} - \frac{(C+6\,D)^2}{C\left(P + 6\sqrt{6}\,R\right)^{1/3}} - \frac{\left(P + 6\sqrt{6}\,R\right)^{1/3}}{C} \quad \text{and} \quad M =$$

$$1 - \frac{6\,D}{C} + \frac{(C+6\,D)^2}{C\left(P + 6\sqrt{6}\,R\right)^{1/3}} + \frac{\left(P + 6\sqrt{6}\,R\right)^{1/3}}{C}$$

$$\frac{\Delta\beta}{\beta} = \Big(-7\,C^7 + C^6\,(702\,D - 3088\,E - 7\,F) + 16\sqrt{6}\,D\,(D - 2\,E)\,F\,(6\,D + F)\,R - C^5\,\left(5892\,D^2 + 28\,224\,E^2 + 3352\,E\,F - 4\,D\,(9376\,E + 189\,F) + 7\,V\right) - 2\,C^4\,\Big(-4156\,D^3 + 16\,D^2\,(3830\,E + 129\,F) + 21\sqrt{6}\,R + 4\,E\,\left(31\,104\,E^2 + 2448\,E\,F - 31\,V\right) + D\,\left(-164\,160\,E^2 - 13\,952\,E\,F + 51\,V\right)\Big) + 2\,C^3\,\Big(25\,776\,D^4 + 16\,D^3\,(-11\,052\,E + 55\,F) - 192\sqrt{6}\,E\,R - 23\sqrt{6}\,F\,R + 1152\,E^2\,V + 2\,D^2\,\left(91\,584\,E^2 - 8080\,E\,F + 165\,V\right) + 8\,D\,\left(2304\,E^2\,F + 27\sqrt{6}\,R - 185\,E\,V\right)\Big) - 4\,C\,\Big(-29\,376\,D^6 - 144\,D^5\,(-264\,E + 17\,F) - 2\sqrt{6}\,D^2\,(528\,E - 53\,F)\,R + \sqrt{6}\,D\,F\,(-128\,E + 7\,F)\,R - 8\sqrt{6}\,E\,R\,V + 24\,D^4\,(132\,E\,F + 17\,V) + 48\,D^3\,\left(17\sqrt{6}\,R - 11\,E\,V\right)\Big) - 4\,C^2\,\Big(-23\,760\,D^5 + 108\,D^4\,(496\,E + 19\,F) + \sqrt{6}\,R\,\left(864\,E^2 + 68\,E\,F - V\right) - 2\,D^3\,\left(15\,552\,E^2 + 1728\,E\,F + 157\,V\right) + 4\,D^2\,\left(864\,E^2\,F + 63\sqrt{6}\,R - 26\,E\,V\right) - 2\,D\,\left(480\sqrt{6}\,E\,R + 41\sqrt{6}\,F\,R - 288\,E^2\,V\right)\Big)\Big) \Big/ \left((3\,C - 12\,D + 8\,E)^2\,V\,\left(C^2 + 36\,D^2 - 6\,D\,F + C\,(12\,D + F) + V\right)\right)$$

where

$$P = C^3 - 108\,C\,D^2 - 216\,D^3 + C^2\,(-90\,D + 432\,E),$$

$$R = \sqrt{-C^2\,(C - 36\,(D - 6\,E))\,\left(2\,C\,D^2 + 4\,D^3 + C^2\,(D - 4\,E)\right)} \quad \text{and} \quad V = \left(P + 6\sqrt{6}\,R\right)^{2/3}$$

REFERENCES

Aki, K., and P. G. Richards, 2002, Quantitative Seismology (second edition): University Science Books.

Bevington, P. R., and D. K. Robinson, 2003, Data Reduction and Error Analysis for the Physical Sciences: McGraw-Hill Higher Education.

Bortfeld, R., 1961, Approximations to the reflection and transmission coefficients of plane longitudinal and transverse waves: Geophys. Prosp., **09**, 485–502.

Brown, A. R., 2004, Interpretation of three dimensional seismic data: AAPG Memoir 42, SEG Investigation in Geophysics, No 9.

Castagna, J. P., and M. M. Backus, eds., 1993, Offset-Dependent Reflectivity - Theory and Practice of AVO analysis: Society of Exploration Geophysicists.

Castagna, J. P., M. L. Batzle, and R. L. Eastwood, 1985, Relationships between compressional-wave and shear-wave velocities in clastic silicate rocks: Geophysics, **50**, 571–581.

Coulombe, C., R. Stewart, and M. Jones, 1992, AVO analysis of VSP and well log data: Technical report, CREWES Research Report, Volume 4.

———, 1996, AVO processing and interpretation of VSP data: Canadian Journal

of Exploration Geophysics, **31**, 41–62.

Donati, M., and N. Martin, 1998, A comparison of approximations for the converted-wave reflection: Technical report, CREWES Research Report Volume 10.

Hampson, and Russell, 2004, AVO theory: Hampson-Russell Software Services Ltd.

Hardage, B. A., 2000, Vertical Seismic Profiling: Principles (second edition): Pergamon.

Muskat, M., and M. W. Meres, 1940, Reflection and transmission coefficients for plane-waves in elastic media: Geophysics, **05**, 115–148.

Ostrander, W. J., 1984, Plane-wave reflection coefficients for gas sands at nonnormal angles-of-incidence: Geophysics, **49**, 1637–1648.

Shuey, R. T., 1985, A simplification of the Zoeppritz-equations: Geophysics, **50**, 609–614. (Errata in GEO-50-9-1522).

Stewart, R. R., J. Gaiser, R. J. Brown, and D. C. Lawton, 2002, Converted-wave seismic exploration: Methods: Geophysics, **67**, 1348–1363.

Stoer, J., and R. Bulirsch, 1993, Introduction to Numerical Analysis: Springer.

Xu, Y., and J. Bancroft, 1997, Joint analysis of PP and PS seismic data: Technical report, CREWES Research Report, Volume 9.

Afeez K. Popoola

Flat 5B Road 3, Owode Housing Estate, Apata, Ibadan, Nigeria

popoolakola@gmail.com, akpopoola@kfupm.edu.sa

(966)548385800/(234)8065525097

Education

M.S., Geophysics *2011 - 2014*

King Fahd University of Petroleum & Minerals (KFUPM) , Dhahran, Saudi Arabia

B.S., Applied Geophysics *November 2009*

Obafemi Awolowo University, Nigeria

Diploma, Computer Science *December 2005*

Federal Polytechnic Ede, Nigeria

Work Experience

Research Assistant, King Fahd University of Petroleum & Mineral, Earth Sciences Department, Saudi Arabia *2011- Present*

Assistant Geophysicist, TINACON Nig. Ltd,Lagos, Nigeria *2009 - 2011*

Skills

Seismic Processing (Surface and VSP), Seismic Interpretation, Well-Log Interpretation & Geostatistics

Seismic Interpretation, Processing and Modeling Softwares: Petrel, OpendTect, PetroMod, Seismic Un*x, Madagascar, Tesseral and SGeMS

Computer Programming: MATLAB, Python, MATHEMATICA,FORTRAN, Bash Shell Scripting

Operating Systems:Linux and Windows

Awards and Honors

Travel Grant, SEG/Chevron Student Leadership Symposium (SLS), 83^{rd} SEG annual meeting, Houston, Texas. *2013*

Gold Medalist, American Association of Petroleum Geologists (AAPG) Imperial Barrel Award (IBA) *2012*

Research Assistantship, Earth Sciences Department KFUPM, Saudi Arabia. 2011

Leadership Activities

President, Society of Exploration Geophysicist (SEG) KFUPM Student chapter, Current

Secretary, American Association of Petroleum Geologists (AAPG), KFUPM student chapter, 2012.